Turing Bifurcations and Pattern Selection

4 authors, including:

P. Borckmans
Université Libre de Bruxelles
122 PUBLICATIONS   **3,168** CITATIONS

SEE PROFILE

Anne De Wit
Université Libre de Bruxelles
237 PUBLICATIONS   **6,761** CITATIONS

SEE PROFILE

Some of the authors of this publication are also working on these related projects:

Project   Self-organisation in reaction-diffusion systems View project

Chemical Waves and Patterns

Raymond Kapral and Kenneth Showalter (Eds.)

CHEMICAL WAVES AND PATTERNS

Understanding Chemical Reactivity

Volume 10

CHEMICAL WAVES

AND PATTERNS

Edited by

RAYMOND KAPRAL

*Department of Chemistry, University of Toronto,
Toronto, Ontario, Canada*

and

KENNETH SHOWALTER

*Department of Chemistry, West Virginia University,
Morgantown, WV, U.S.A.*

Library of Congress Cataloging-in-Publication Data

Printed on acid-free paper

10. Turing Bifurcations and Pattern Selection

P. BORCKMANS, G. DEWEL, A. DE WIT and D. WALGRAEF
Service de Chimie-Physique/Center for Nonlinear Phenomena and Complex Systems, CP 231, Université Libre de Bruxelles, 1050 Bruxelles, Belgium

1. Introduction

Pattern forming instabilities in spatially extended dissipative systems driven away from equilibrium have been the focus of a large activity for many years. The goal of this chapter is to present some theoretical concepts that have been developed to understand and describe these *dissipative structures* [1] from a macroscopic point of view. Although these methods present generic features we shall only be concerned with chemical patterning and shall not discuss here instabilities in hydrodynamics, liquid crystals and nonlinear optics that all present similar types of organization because the latter have been the subject of recent well-documented reviews [2–5]. Moreover, we essentially consider the self-organization of structures discarding the spatial patterning resulting from boundary conditions.

The systems which will be discussed in this paper present some type of positive feedback loop initiated by an activator which promotes its own production and is controlled by an inhibitor to which a negative feedback is associated. The dissipative structures can form when the inhibition is of longer range than the activation process. This allows the local growth of the activator while the lateral inhibition prevents the spreading of the activated center. Such a process will repeat itself finally leading to a stationary pattern. The spatial decoupling between the two processes takes different forms in various systems.

In his study of the cellular structure of flames, Zeldovich [6] is among the first who has stressed the importance of this mechanism. He has indeed shown that a plane flame front can undergo an instability if the diffusivity of the species limiting the reaction (inhibitor) exceeds the thermal diffusivity (activator) of the gas mixture.

On the other hand, Rashevsky [7] and Turing [8] have shown that the homogeneous steady states of *isothermal* reaction-diffusion systems can also be destabilized by perturbations of finite wavenumber as some control parameter is varied. Chemical species involved in stable nonlinear chemical reactions may thus organize spontaneously in space through differential diffusive processes. The beauty of Turing's idea lies in this counterintuitive organizing

role of diffusion that usually tends to smear out any concentrations inhomogeneity. The term *diffusion driven instability* has been coined to characterize this important mechanism. After Prigogine and collaborators [9] had shown that this instability is not in contradiction with basic thermodynamic principles, it has been proposed as the paradigm for modelling spatial symmetry breaking instabilities in chemistry and biology [10, 11]. In the second case it has been successfully applied to explain the onset of chemical prepatterns in developmental biology. There also the diffusion coefficients of the autocatalytic species must be smaller than that of their antagonists, the inhibitors. It is precisely this condition that for forty years has prevented the experimental observation of this instability in simple isothermal chemical systems.

Thereafter it has been stressed that the mechanism of diffusion driven instability is pertinent to the formation of dissipative structures in other fields: electron-hole plasmas in semiconductors [12], gas discharge devices [13], semiconductor structures (p-n junction, p-i-n diodes) [14], heterogeneous catalysis [15], materials irradiated with energetic particles or light [16–18], ...

All these physically different systems can formally be cast in a common language. However since it is the recent experimental observations [19, 20] of Turing patterns that has induced a renewed interest in diffusion driven instabilities, in the following, we mainly discuss the case of the Turing instability in reaction-diffusion systems.

2. Turing Instability

For the sake of completeness we briefly recall some basic features about the pattern forming Turing instability. The standard reaction-diffusion equations can be written in the form

$$\frac{\partial \mathbf{C}}{\partial t} = \mathbf{F}(\mathbf{C}; B) + \mathbf{D}\nabla^2 \mathbf{C}. \tag{1}$$

Appropriate initial and boundary conditions should also be added to complete the mathematical formulation. In Equation (1) $\mathbf{C}(\mathbf{r}, t)$ is the local concentration vector, $\mathbf{F}(\mathbf{C}; B)$ a vector function representing the reaction kinetics, B stands for a set of control parameters and $\mathbf{D}$ is the matrix of transport coefficients. In most chemical systems involving small molecules in aqueous solutions, the diffusion processes are well described by a diagonal matrix with constant positive diffusion coefficients. However, in some systems it is the coupling between the transport processes that provides the engine of the instability. For instance, stratification occurs in electron-hole plasmas in semiconductors subjected to electromagnetic radiations because of the effect of the temperature field on the carrier density distribution (thermodiffusion)

[21]. Similarly cross-diffusion effects play an important role in chemotaxis in biology [11], i.e. the aggregation of cells or insects induced by some chemical attractant. Along with the development of the field important variations in the standard Equation (1) have been introduced. Let us merely cite three such examples. In developmental biology the role played by the mechanical forces in the process of morphogenesis has been taken into account in the mechanochemical models [11]. In order to sustain the chemical structures fresh reactants must continuously be supplied. The interaction of the resulting hydrodynamic flows with chemical instabilities has been described by reaction-diffusion-convection models where an advection terms $\mathbf{v} \cdot \nabla \mathbf{C}$ must be added in Equation (1) if the chemistry is passive with respect to the flow. Finally, all systems cannot be described in the framework of a spatially local dynamics [22]. This happens when the dynamical behavior is dominated by long range effects. Equation (1) must then be replaced by partial integro-differential equations which for instance take the form:

$$\frac{\partial \mathbf{C}}{\partial t} = \mathbf{F}(\mathbf{C}, B) + \int d\mathbf{r}' \mathbf{K}(|\mathbf{r} - \mathbf{r}'|) \mathbf{C}(\mathbf{r}', t) \tag{2}$$

where the kernel, which depends only on the distance $|\mathbf{r} - \mathbf{r}'|$, describes the effect of the neighboring $\mathbf{C}(\mathbf{r}', t)$ on $\mathbf{C}(\mathbf{r}, t)$. In other systems such as electrically heated catalytic ribbons [23], gas discharges [13] or the ballast resistor [24] an integral constraint plays the role of the inhibitor and can generate nontrivial patterns even in one-variable systems.

Consider a homogeneous steady state (HSS) $\mathbf{C}_0$ of Equation (1), such that $\mathbf{F}(\mathbf{C}_0) = 0$, stable in the corresponding well-stirred reactor. In an unstirred reactor one then investigates the fate of a small amplitude inhomogeneous perturbation $\mathbf{u}(r, t) = \mathbf{C}(r, t) - \mathbf{C}_0$ by applying the standard *linear stability analysis*. One writes

$$\mathbf{u}(\mathbf{r}, t) = \sum_n \mathbf{c}_n \, e^{\omega_n t} \Phi_n(\mathbf{r}) \tag{3}$$

where the $\Phi_n(\mathbf{r})$ satisfy

$$\nabla^2 \Phi_n(\mathbf{r}) = -k_n^2 \Phi_n(\mathbf{r}) \tag{4}$$

for the given boundary conditions.

Substituting (3) into (1) leads after linearization to the following eigenvalue problem

$$\|\mathbf{L} - \mathbf{D}k^2 - \mathbf{I}\omega\| = 0 \tag{5}$$

where $\mathbf{L}$ is the Jacobian matrix. A diffusion driven instability occurs when for the first time a single eigenvalue $\omega(k)$ crosses the imaginary axis for some nonzero $k \, (= k_c)$ with $\text{Im}(\omega(k_c)) = 0$. At this point the equation

$$\|\mathbf{L} - \mathbf{D}k^2\| = 0 \tag{6}$$

has a strictly positive degenerate root k_c^2, i.e.

$$\left. \frac{\mathrm{d}\|\mathbf{L} - \mathbf{D}k^2\|}{\mathrm{d}k^2} \right|_{B_c, k_c} = 0. \tag{7}$$

These two conditions, Equations (6) and (7), allow us to determine the threshold B_c and the critical wavelength $\lambda_c = 2\pi/k_c \propto (D_h D_a)^{1/2}$, where D_h and D_a are the inhibitor and activator diffusion coefficients if one considers a two variable model.

If there is more than one wavevector satisfying these conditions we have a degeneracy. The nature of the spectrum of the Laplacian operator strongly depends on the aspect ratio, i.e. the ratio of the characteristic size of the reactor to the critical wavelength of the instability. In low aspect ratio systems, the spectrum is discrete and at most finitely degenerate [1, 2, 11]. This degeneracy is usually related to the symmetry properties of the geometry of the reactor. Near B_c then, only a finite number of eigenvalues have crossed the imaginary axis; the boundaries then play a major role in isolating specific wavelengths. On the contrary in spatially extended systems the distance between nearest eigenvalues is so small that for all practical purposes the domain can effectively be considered as infinite leading to a continuous spectrum. The experimental Turing structures [19, 20] which involve hundreds of wavelengths clearly belong to this class. In these systems all the wavevectors lying on the critical manifold $|\mathbf{k}| = k_c$ are equally amplified. Near threshold the growth rate of the critical modes indeed takes the form:

$$\omega(k) = \mu - \xi_0^2 (k^2 - k_c^2)^2 / 4k_c^2 \tag{8}$$

where $\mu = (B - B_c)/B_c$ measures the distance from the instability point and ξ_0 is the coherence length of order k_c^{-1}. This infinite degeneracy is the reflection of the *rotational symmetry* exhibited by spatially extended systems. Therefore the pattern that will finally emerge cannot uniquely be determined by the linear stability analysis.

This orientational degeneracy is of course raised in anisotropic systems such as in the case of the patterns formed during catalysis at single crystal surfaces [25] or in metals under irradiation [16–18]. The diffusion coefficients of some species are then highest along some crystallographic directions. In a 2D uniaxial medium the reaction-diffusion equations are now:

$$\frac{\partial \mathbf{C}}{\partial t} = \mathbf{F}(\mathbf{C}; B) + \mathbf{D}_x \frac{\partial^2 \mathbf{C}}{\partial x^2} + \mathbf{D}_y \frac{\partial^2 \mathbf{C}}{\partial y^2} . \tag{9}$$

This anisotropy in the transport coefficients induces preferred directions for the critical wavevectors and these solutions appear already in the linear analysis. The growth rate now for instance takes the form

$$\omega(k) = \mu - \xi_0^2 (k^2 - k_c^2)^2 / 4k_c^2 - \mathcal{A}k^2 \sin\phi \tag{10}$$

$\mathcal{A} > 0$ is a constant characterizing the anisotropy and ϕ is the angle made by the wavevector with the direction of the easy axis. In the case of the Turing instability, the easy axis corresponds to the direction along which the ratio of the diffusion coefficients of the activator and the inhibitor is the smallest [26].

On the other hand, as soon as $B > B_c$ a continuous band of unstable wavenumbers appears for each direction. The width of this band, $|\mathbf{k}| = k_c + Q$, is obtained from Equation (8) where

$$-\sqrt{\mu}/\xi_0 \leq Q \leq \sqrt{\mu}/\xi_0. \tag{11}$$

For systems with an infinite support all the modes in an annulus (2D) or a spherical shell (3D) of width $2\sqrt{\mu}/\xi_0$ bracketing the critical manifold are excited. The existence of such continuous *sidebands* makes it more difficult to rigorously define an order parameter for spatially extended systems. For most systems this width increases when the diffusion coefficient of the activator is decreased at constant μ. In the limiting case $D_a \to 0$ (immobilized activator) the spectrum is unbounded at large wavenumbers: the homogeneous steady state can be destabilized by any perturbation, with a wavenumber larger than $k_{min} \propto 1/\sqrt{D_h}$. We shall not discuss this limiting case where the wavelength degeneracy may lead to a large multiplicity of patterns even in one-dimensional systems [27].

3. Pattern Selection in the Weakly Nonlinear Regime

The linear stability analysis of the reference state has determined the critical value B_c of the control, or stress, parameter, B, above which various modes with wavevector near k_c begin to grow exponentially leading eventually to new patterned solutions of the problem. In this section we are interested in what shapes are selected for values of B near B_c.

3.1. GENERAL PRINCIPLES

The principles of this study may be outlined in three steps.

3.1.1. Determination of the Active Modes

The *active modes* are those responsible for the loss of stability of the reference state by growing exponentially. They do so by drawing on the imposed driving force and thus end up competing nonlinearly to create the new solutions. In large aspect ratio systems as those characterizing the recent experiments, we have noticed in the preceding section that we face a large degeneracy of destabilizing modes (rotational invariance and existence of sidebands) as

soon as the stress parameter exceeds its critical bifurcation value. Therefore the pattern that will emerge is not uniquely defined by the results of the linear stability analysis as for small aspect ratio systems where the roots of the dispersion relation are discrete, at most weakly degenerate. The pattern selection problem is thus made much more accute because of the existence of this large multiplicity of possible solutions.

On the other hand, there exist so-called *passive modes*, the linear frequencies of which are still damped above B_c. They however also come into the determination of the pattern as they are continuously regenerated by the non-linear interactions between members of the active set. Their dynamics results from the balance between this regeneration and their rapid linear decay. Their amplitudes may therefore be algebraically related to those of the active modes as a result of an adiabatic elimination process that is reminiscent of the Bodenstein stationarity approximation. They are therefore often termed 'slaved' modes as they feed on the stress source only through active modes.

3.1.2. Amplitude Equations for the Active Modes

There exist standard bifurcation techniques [1, 2, 28] that allow one to obtain evolution equations for the *amplitudes* of the active modes or *order parameters* as they are often called because they determine the degree of order in the system. We now sketch the principles of this derivation referring the reader to typical reviews on the subject for the technical details. Near threshold, B_c, one proceeds by expanding the difference of the concentration field $\mathbf{C}(\mathbf{r}, t)$ from its reference state $\mathbf{C}_0$ as an asymptotic series

$$\mathbf{C}(\mathbf{r}, t) - \mathbf{C}_0 = \varepsilon \mathbf{C}_1 + \varepsilon^2 \mathbf{C}_2 + \varepsilon^3 \mathbf{C}_3 + \cdots \tag{12}$$

where the small expansion parameter ε is related to the distance μ from threshold by

$$\mu \propto B - B_c = \varepsilon B_1 + \varepsilon^2 B_2 + \varepsilon^3 B_3 + \cdots \tag{13}$$

and $\mathbf{C}_1$ is a linear combination of the active modes. Now, it is known from linear stability analysis, that for large aspect ratio systems, one has to take care of two kinds of degeneracies in the determination of the active modes. The rotational degeneracy may be tackled first, ignoring in this step, the effects arising from the presence of sidebands. At the leading order of approximation one writes

$$\varepsilon \mathbf{C}_1 = \mathbf{E}_\mathrm{T} \sum_{i=1}^{M} [A_i(T)\, e^{i\mathbf{k}_i \cdot \mathbf{r}} + c \cdot c] \tag{14}$$

where $\mathbf{E}_\mathrm{T}$ is the critical eigenvector of the linear evolution operator and we consider complex amplitudes A_i to take the translational invariance of the

infinite system into account. The set of M pairs of wavevectors $\{k_i, -k_i\}$ characterizing the active modes are chosen on the critical circle (2D) or sphere (3D), $|\mathbf{k}| = k_c$ in k-space. Because concentrations are real the active modes must involve pairs of opposite wavevectors. Each set defines a possible pattern – e.g. in 2D: stripes ($M = 1$), rhombs ($M = 2$), hexagons ($M = 3$) or even quasicrystalline structures ($M > 3$) – and the amplitude equations we have set out to obtain will determine what pattern is favored by the nonlinear interactions. The amplitudes A_i depend on the natural slow time scale of the critical mode that is proportional to $1/\mu$ ($T = \mu t$). The higher order corrections $\{\mathbf{C_n}\}$ ($n > 1$) are then determined by substituting the expansions (13) and (14) in the nonlinear reaction-diffusion equations. Equating the successive powers of ε leads to a set of linear inhomogeneous equations that are solved recursively. The solvability conditions of these inhomogeneous equations (Fredholm alternative theorem) then lead to a set of ODEs: the *amplitude equations* for the active modes

$$\frac{\mathrm{d}A_i}{\mathrm{d}t} = \mu A_i + G_i(\{A_j\}) \tag{15}$$

where $G_i(\{A_j\})$ are nonlinear polynomials in the active amplitudes. These equations are universal in character and the information concerning a particular system is solely contained in the structure of the polynomials and their coefficients.

Once the forms of the possible solutions have been obtained, we may take into account the second degeneracy related to the existence of the sidebands of modes that also interact nonlinearly with the critical modes. Therefore one could generalize Equation (14) and write for *each term* of the sum over index i an infinite sum over the contributions from all wavevectors lying in the sidebands

$$\sum_\alpha \left[A_{i,\alpha}(T)\, e^{i(\mathbf{k_i}+\mathbf{Q_\alpha})\cdot\mathbf{r}} + c \cdot c \right] \quad |\mathbf{k_i}| = k_c \tag{16}$$

where the $\mathbf{Q}_\alpha$ denote the modes in the sidebands in the vicinity of $\mathbf{k_i}$.

However the sum over α in Equation (16) can be more simply written as

$$A_i \left(X_i = \sqrt{\mu}\, x_i, Y_i = \sqrt[4]{\mu}\, y_i, Z_i = \sqrt[4]{\mu}\, z_i; T = \mu t \right)\, e^{i\mathbf{k_i}\cdot\mathbf{r}} + c \cdot c \tag{17}$$

where X_i lies in the direction of $\mathbf{k_i}$ and (Y_i, Z_i) span the plane orthogonal to this direction. Equation (17) not only includes Equation (14) as a special case, but also the contributions from the full band of modes. The argument of A_i in Equation (17) characterizes the vicinity mentioned before. Note however that in the case of structures involving resonant interactions, e.g. as for hexagons ($M = 3$) in 2D, the length scaling should remain isotropic [128].

Thus the envelopes $A_i(R, T)$ of the various short scale (k_c^{-1}) mode shapes have now been introduced as order parameters. They express the beating of all modes in the sidebands with the critical mode and thereby allow for modulations of the amplitudes A_i over distances of $1/\sqrt{\mu}$ times the coherence length.

Proceeding along similar lines as before one obtains the *envelope amplitude equations* that are now PDEs that describe the nonlinear interactive behaviour of the wavepackets accounting for the dynamics of all the modes included in the annulus (2D) or spherical shell (3D) of width $2\sqrt{\mu}/\xi_0$ in k-space:

$$\frac{\partial A_i}{\partial t} = \mu A_i + G_i(\{A_j\}) + \xi_0^2 \Box^2 A_i \tag{18}$$

Here $\Box$ is a spatial operator describing the modulation of the patterns on the extended length scale. Its precise form depends on the presence, or not, of resonant couplings in $G_i(\{A_j\})$ [128].

These equations thus allow for the description of the large scale nonuniformities of the patterns.

3.1.3. Determination of the Stable Patterns – Bifurcation Diagram

As the resulting amplitude equations, Equation (15), have a lower dimension they are simpler to analyze than the original reaction-diffusion systems [Equation (1)] remembering however that they are only valid in some neighbourhood of the point where the reference state linearly looses its stability. Because of this relative simplicity they allow to scrutinize the key nonlinear effects that govern the structure of the bifurcation diagram. In the first place however they allow one to obtain the bifurcated solutions and to discuss their stability.

The investigation of the stability is again carried out through linear stability analysis, now however around the newly bifurcated state. The difficulty in the analysis arises from the fact that for each state one has to discuss the stability with respect to *all* possible types of perturbations: amplitude, modulus and orientation of the wavevector and also resonant perturbations to other structures with different symmetries.

A further complication is provided by the large number of coexisting stable solutions as their relative stability must then be decided upon. Near the bifurcation ($\mu = 0$) leading to the formation of Turing patterns, the amplitude equations are relaxational (this may however not be the case of the envelope amplitude equations) in their structure and can thus be derived

from a Lyapunov functional $\mathcal{L}[A, A^*]$ such that

$$\frac{\partial A_i}{\partial t} = -\frac{\delta \mathcal{L}[A, A^*]}{\delta A_i^*} \tag{19}$$

where $\mathcal{L}[A, A^*]$ decreases monotonously in time during the evolution of the system

$$\frac{\partial \mathcal{L}}{\partial t} = -\sum_i \left(\frac{\delta \mathcal{L}}{\delta A_i^*} \right)^2 \leq 0. \tag{20}$$

Therefore the *globally stable* pattern corresponds, for given μ, to the absolute minimum of $\mathcal{L}[A, A^*]$, whereas the relative minima represent *metastable* structures that arise when multistability is present. The maxima naturally represent *unstable* states.

However, to test the relative stability of simultaneously stable states in the variational case another means is available. It amounts to considering the velocity, v, of a *front* (domain wall) joining two bistable solutions (say $\mathcal{A}_1$ and $\mathcal{A}_2$) of the amplitude equations. If for $\mu_1 \leq \mu \leq \mu_2$ these two states are bistable, then there exists a single value μ_{co} in this interval for which the front is stationary ($v = 0$) and the solutions $\mathcal{A}_1$ and $\mathcal{A}_2$ coexist in space. For all other values in the interval $\{\mu_1, \mu_2\}$ one solution will dominate the other and invade the whole system. This state is then the stablest. As in classical nucleation theory, droplets of one state imbedded in the other are then always unstable. Those with a radius smaller than some given critical radius will shrink away while those with a radius larger than critical will fill up the whole system. The problem of stability of a front or a droplet is even trickier in the case considered in this review because one deals with states that possess their own intrinsic characteristic length ($\approx k_c^{-1}$). It is then well known that the fronts may become pinned ($v = 0$) because of their interaction with the underlying Turing structure [29]. The droplets resulting from the juxtaposition of such fronts may then be stabilized (see Section 5).

However, the chemical systems we are interested in hardly ever exhibit such gradient or variational properties, except in the close neighbourhood of the instability point. The above picture is then soon lost as the distance from the bifurcation point increases. When the system does not possess gradient properties even the method of fronts is not available to test the relative stability of solutions $\mathcal{A}_1$ and $\mathcal{A}_2$ as for a given value of the parameters one can have fronts going in either direction [30]. The nonvariational terms may furthermore give rise to new interactions between fronts also leading to stable droplets [31].

3.2. ILLUSTRATIONS

3.2.1. Space Dimension = 1

Although there is no experimental implementation of this case without the presence of a ramp of some parameter, it is the simplest to treat theoretically as the orientational degeneracy discussed previously is not present. One has thus only to consider the case $M = 1$ in Equation (14), i.e.:

$$\varepsilon \mathbf{C}_1 = \mathbf{E}_T \left[A_1(T) \, e^{i\mathbf{k}_1 \cdot \mathbf{r}} + c \cdot c \right].$$

At the lowest order, the amplitude equation reads

$$\frac{dA_1}{dt} = \mu A_1 - g_D |A_1|^2 A_1 \tag{21}$$

where the g_D coefficient expresses the strength of the self-nonlinear interaction of the active mode that is characteristic of the particularities of the specific chemical system considered.

The stationary solutions of Equation (21) are:
- uniform reference state: $A_{1,s} = 0$
- stripes perpendicular to $\mathbf{k}_1$: $A_{1,s} = \sqrt{\mu/g_D} \, e^{i\phi}$
  so that the concentration field in the new bifurcated state reads (if $\mathbf{k}_1 \parallel \mathbf{1}_x$)

$$\mathbf{C} = \mathbf{C}_0 + 2\mathbf{E}_T \sqrt{\frac{\mu}{g_D}} \cos(k_c x + \phi). \tag{22}$$

It corresponds to a periodic modulation of the concentrations along the system. Here ϕ is the phase of the pattern that may be set to zero by a suitable choice of the coordinates. Truly, as we have already argued, as soon as $\mu > 0$, in an extended system a whole band of periodic states with a wavenumber near k_c (sidebands) bifurcate simultaneously. These are solutions of the envelope amplitude equations and will be discussed in Section 4.

Bearing in mind that the reference solution exists for all values of μ, two subcases are to be distinguished: if $g_D > 0$, the bifurcation is *supercritical* as the new solution exists for $\mu > 0$; whereas if $g_D < 0$ the new solution arises for $\mu < 0$ and the bifurcation is said to be *subcritical*. In both cases we have a pitchfork bifurcation (see Figures 1a, b).

As mentioned in the preceding section, once the bifurcating solutions have been determined, one has to test their stability by resorting again to linear stability analysis with respect to the new solution ($A_1 = A_{1,s} + \delta A_1$). These are perturbations of the modulus; the stability with respect to modifications of the wavenumber will be considered later. For $\mu > 0$, the trivial solution $A_{1,s} = 0$ is obviously unstable while the new solution is stable in the supercritical case. However, the reverse is true in the subcritical case. For $\mu > 0$ no stable
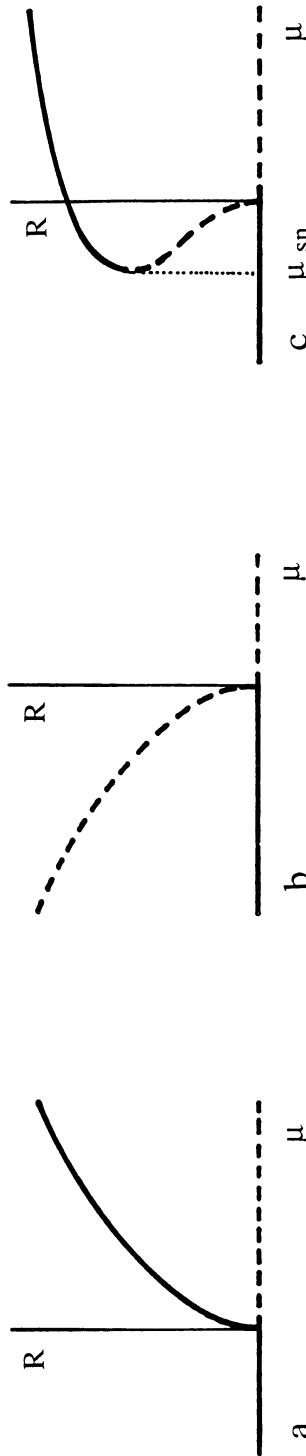
Fig. 1. Schematic bifurcation diagrams in the amplitude (modulus R)/bifurcation parameter (μ) representation: (a) supercritical case; (b) subcritical case; (c) saturated subcritical case, where the stable nonlinear branch of solutions appears with a finite amplitude at a secondary saddle-node bifurcation (μ_{sn}). Thick (broken) lines indicate stable (unstable) branch of solutions.

solution exists, whereas the nonlinear solution is unstable for $\mu < 0$: the instability has not been saturated. The bifurcation calculation must then be carried out to the next order that yields the following amplitude equation

$$\frac{\mathrm{d}A_1}{\mathrm{d}t} = \mu A_1 - g_D |A_1|^2 A_1 - g_D' |A_1|^4 A_1 \qquad (g_D < 0). \tag{23}$$

If g_D' is now positive (otherwise one has to go on with the procedure) the bifurcation saturates leading to the bifurcation diagram given in Figure 1c that now also involves a secondary saddle-node bifurcation [2] for $\mu_{sn} = -g_D^2/4g_D'$. The stability of the various branches are then calculated in standard fashion. For $\mu_{sn} < \mu < 0$, one has bistability between the periodic structured state and the trivial uniform state with the possibility of observing localized structures (see Section 5).

3.2.2. Space Dimension = 2

The effect of the orientational degeneracy has now to be taken into account as all the modes lying on the *critical circle* $|\mathbf{k}| = k_c$ may become unstable. The existing techniques imply that we tackle the case of each value of M in turn.

For $M = 1$, we have structures periodic in one direction, *stripes*, in our 2D space. The nature of the solutions and of the bifurcations are as in 1D. However the stability problem now also implies testing the stability of the stripes with respect to the formation of patterns of other symmetries. As shown in Section 4, other wavenumber modulational instabilities may also occur as compared to the 1D situation.

For larger M, one usually restricts oneself to patterns obtained by regularly superposing [32] M pairs of 'modes with' wavevectors that make angles multiples of π/M with each other because of the isotropy of the nonlinear couplings in the reaction-diffusion system.

The $M = 2$ case corresponds to *squares*. If the concentration field is written ($\mathbf{k}_1 \perp \mathbf{k}_2$),

$$\varepsilon \mathbf{C}_1 = \mathbf{E}_{\mathbf{T}} \left[A_1(T) \, \mathrm{e}^{i\mathbf{k}_1 \cdot \mathbf{r}} + A_2(T) \, \mathrm{e}^{i\mathbf{k}_2 \cdot \mathbf{r}} + c \cdot c \right],$$

the amplitude equations read

$$\frac{\mathrm{d}A_1}{\mathrm{d}t} = \mu A_1 - g_D |A_1|^2 A_1 - g_{ND} |A_2|^2 A_1$$

$$\frac{\mathrm{d}A_1}{\mathrm{d}t} = \mu A_2 - g_D |A_2|^2 A_2 - g_{ND} |A_1|^2 A_2. \tag{24}$$

They now involve self (D) as well as cross (ND) nonlinear couplings among the active modes and we have limited ourselves to the case where the instability is saturated at this order ($g_D > 0$, $g_{ND} > 0$).

Before proceeding it is worth remarking that since only the cosine of the angle between the wavevectors comes into play, semiregular distributions of wavevectors could also arise if some anisotropy were present, thereby generating, and perhaps favoring *rhombs*.

Four possible solutions emerge from the previous amplitude equations:
 - uniform reference state: $A_{1,s} = 0$, $A_{2,s} = 0$
 - stripes perpendicular to k_1: $A_{1,s} = \sqrt{\mu/g_D}\, e^{i\phi_1}$, $A_{2,s} = 0$
 - stripes perpendicular to k_2: $A_{1,s} = 0$, $A_{2,s} = \sqrt{\mu/g_D}\, e^{i\phi_2}$
 - squares: $A_{1,s} = \sqrt{\mu/(g_D + g_{ND})}\, e^{i\phi_1}$, $A_{2,s} = \sqrt{\mu/(g_D + g_{ND})}\, e^{i\phi_2}$

where the phase factors can be discarded through a convenient choice of the coordinates.

The linear stability of these new supercritical branches is then tested ($A_i = A_{i,s} + \delta A_i$). One finds that if $g_D < g_{ND}$, as is usually the case in isotropic reaction-diffusion problems (heterogeneous catalysis may provide counterexamples), the stripes are stable and the squares unstable. The reverse condition leads to the opposite conclusion. Therefore stripes and squares are mutually exclusive [33]. However no definitive conclusion regarding the stability of the 'winning' state should be drawn as its stability must still be tested with respect to perturbations involving higher values of M. As always their stability should also be checked regarding wavenumber changes (Section 4).

For $M = 3$, where the wavevectors are directed at angles $2\pi/3$ to each other, a resonant condition $k_1 + k_2 + k_3 = 0$ ($|k_1| = |k_2| = |k_3 = k_c$) among a triad of active modes becomes possible. At the lowest order the amplitude equations are

$$\frac{dA_i}{dt} = \mu A_i + v A_{i+1}^* A_{i-1}^* \qquad (i, j = 1, 2, 3) \tag{25}$$

where the indices are defined modulo 3. Two of the three phases can be fixed by the choice of the coordinate system. The third, or equivalently the sum of the three phases, $\phi = \Sigma\phi_i$, is adjusted dynamically. Indeed in terms of the moduli R_i and ϕ, the amplitude equations read

$$\frac{dR_i}{dt} = \mu R_i + v R_{i+1} R_{i-1} \cos\phi$$

$$\frac{d\phi}{dt} = -\sum_{i \neq j} v \frac{R_i^2 R_j^2}{\prod_k R_k} \sin\phi \qquad (i, j = 1, 2, 3). \tag{26}$$

It follows from Equation (26) that ϕ relaxes monotonically to π or 0 according to the sign of v (- or +), the quadratic coupling of the active modes, while the
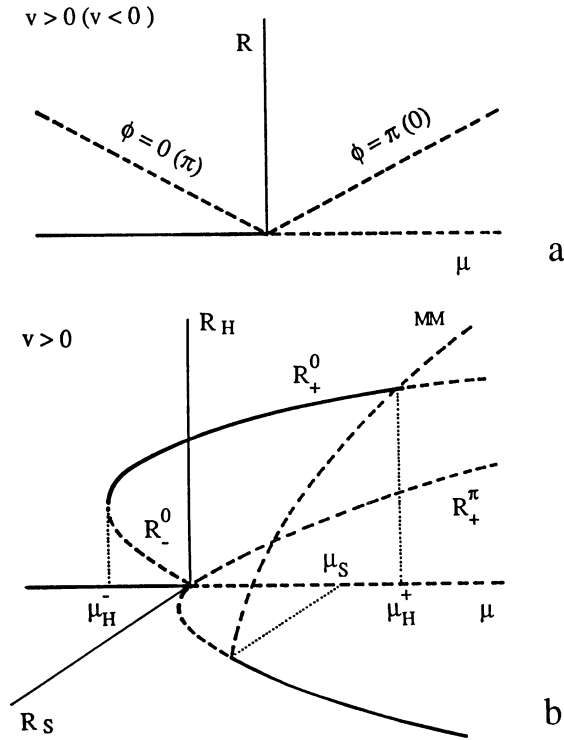
Fig. 2. Schematic bifurcation diagrams in the amplitude (modulus R)/bifurcation parameter (μ) representation: (a) amplitudes of the stationary solutions of hexagonal symmetry as given by Equation (26); (b) amplitudes of both the hexagonal and stripe solutions as given by Equation (27). Thick (broken) lines indicate stable (unstable) branch of solutions.

differences $R_i - R_j$ decay in time giving rise to perturbations with hexagonal symmetry ($R_{1,s} = R_{2,s} = R_{3,s}$).

Accordingly the bifurcated states are, for $v > 0$, $R_{i,s}$ ($i = 1, 2, 3$) $= \pm\mu/v$, where the signs refer respectively to $\phi = 0$ and $\phi = \pi$. The former exists for $\mu < 0$ and is stable with respect to total phase perturbations but unstable to perturbations of its amplitude. The latter, existing for $\mu > 0$, is already unstable to total phase perturbations (Figure 2a). The reverse conclusions, regarding the total phase, holds for $v < 0$. The bifurcation is thus of *transcritical* nature but is not saturated at the order considered. This can be dealt with, as discussed above, by going to a higher order of approximation introducing couplings among a larger number of active modes. The simplest, that we have already met is the cubic coupling. The amplitude equations then become

$$\frac{\mathrm{d}A_i}{\mathrm{d}t} = \mu A_i + v A_{i+1}^* A_{i-1}^*$$

$$- g_D |A_i|^2 A_i - g_{ND} \sum_{i \neq j} |A_j|^2 A_i \qquad (i, j = 1, 2, 3). \qquad (27)$$

Such an equation, with nonlinear terms of mixed order can however only be derived rigorously if the quadratic coupling is sufficiently weak. It brings a secondary saddle-node bifurcation into play.

Equation (27) allows for four types of solutions (the free phase factors have been discarded by the choice of the coordinate system):

- uniform reference state: $R_{1,s} = R_{2,s} = R_{3,s} = 0$. It is stable (unstable) for $\mu < 0$ ($\mu > 0$).
- stripes perpendicular to $\mathbf{k}_1$: $R_{1,s} = \sqrt{\mu/g_D}$, $R_{2,s} = R_{3,s} = 0$ (and permutations when $\perp \mathbf{k}_2$ or $\mathbf{k}_3$). They are stable for $\mu > \mu_s = v^2 g_D/(g_{ND} - g_D)^2$. Below this value the stripes are unstable with respect to the formation of hexagons. Hence the previous word of caution regarding their stability study.
- hexagons: $R_{1,s} = R_{2,s} = R_{3,s} = R_{\pm}^{\phi}$, are the solutions of $(g_D + 2g_{ND})R^2 - v \cos \phi R - \mu = 0$, and $\phi = 0$ or π. For $v > 0$, R_+^{π} exists only for $\mu > 0$ and is always unstable to total phase perturbations. If $\phi = 0$, solutions exist for $\mu > \mu_h^- = -v^2/4(g_D + 2g_{ND})$. The upper branch R_+^0 is stable up to $\mu = \mu_h^+ = v^2(2g_D + g_{ND})/(g_{ND} - g_D)^2$. The lower branch R_-^0 is unstable. The reverse conditions with respect to the total phase hold for $v < 0$.
- mixed modes: $R_{1,s} = U = v/(g_{ND} - g_D)$, $R_{2,s} = R_{3,s}$ $= \sqrt{(\mu - g_D U^2)/(g_D + g_{ND})}$ with $\phi = 0$ for $v > 0$ (and permutations). They exist for $\mu > \mu_s$ and are unstable.

These solutions are represented with their relative stability in Figure 2b.

Therefore, depending on the sign of the quadratic coupling one has either H0 hexagons ($v > 0$ and $\phi = 0$) when the maxima of concentration form a triangular lattice or Hπ hexagons ($v < 0$ and $\phi = \pi$) when the maxima of concentration form a honeycomb lattice. The basic stable patterns are shown in Figure 3.

In the frame of this weakly nonlinear theory the hexagons are the first to appear, subcritically; on increasing the value of the bifurcation parameter μ, the hexagons become unstable with respect to stripes. Reversing the variation of μ allows one to recover the hexagonal structure but by undergoing an hysteresis loop. This is the 'universal' hex-stripes competition scenario that comes up in many different fields of study. It is also that which is observed in the quasi-2D Turing experiments [20, 34] and in the theoretical analysis [35–39] and numerical simulations of most nonlinear chemical models [40–44].

Modifications of this scenario in the vicinity of the primary bifurcation point $\mu = 0$ include the case where the cubic couplings are such that the stripes also arise subcritically. This is for instance the case [43] in a region of
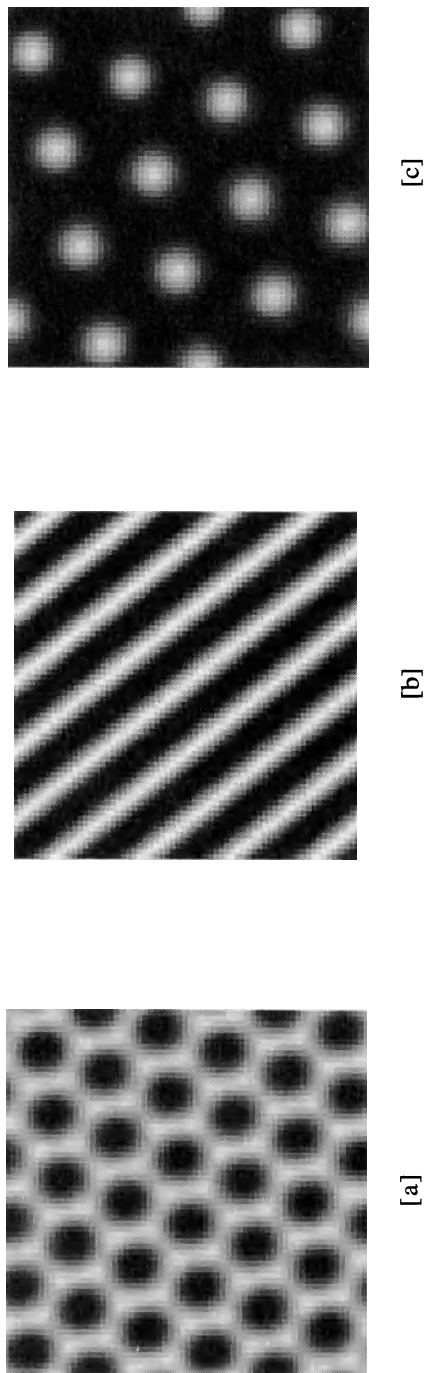
Fig. 3. The three basic 2D patterns for species X of the Brusselator model. The gray scale corresponds to the concentrations lying between the absolute minimum (black) and maximum (white); it thus measures relative concentrations variations with respect to the uniform reference state. The maxima form (a) a honeycomb; (b) stripes; (c) triangles.
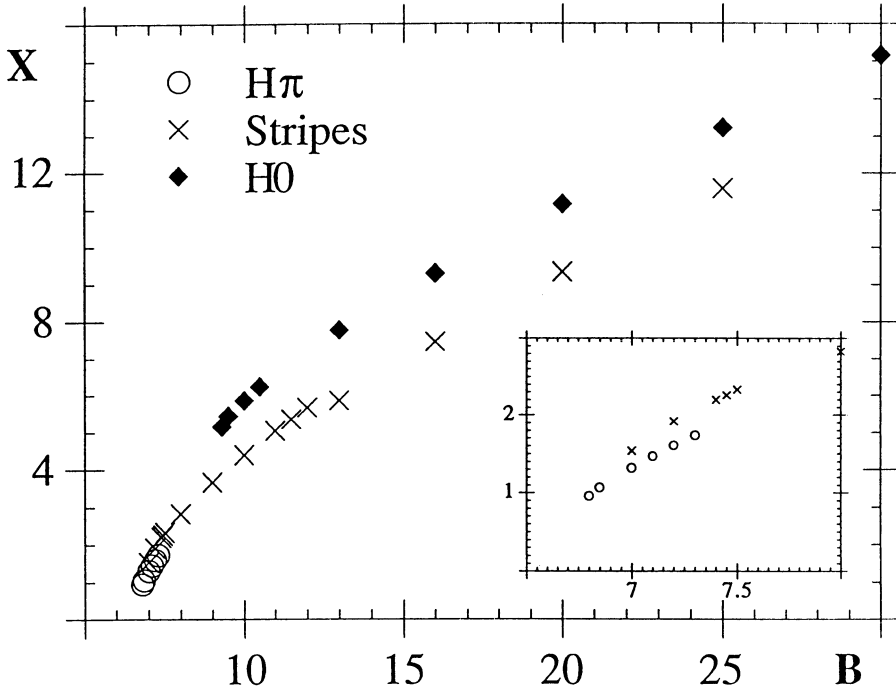
Fig. 4. Bifurcation diagram for variable X of the Brusselator ($A = 4.5$, $D_y/D_x = 8$) as a function of the parameter B. It exhibits the standard hex-stripe competition (hysteresis loop) near the primary bifurcation ($B_c = 6.71$). Reentrant hexagons become stable for higher values of the bifurcation parameter B. $[X_{max} - A]$ is represented.

parameter space for the Lengyel–Epstein model [45]. Furthermore, when the competition is between squares and hexagons ($g_D > g_{ND}$), the squares are unstable (as were the stripes) near $\mu = 0$. As the parameter increases squares and hexagons coexist but thereafter the hexagons never become unstable (no hysteresis loop) [33].

When $v < 0$, if one numerically computes the bifurcation diagram for the Brusselator model [40], one finds, near $\mu = 0$ ($B = B_c$), the hex-stripes competition just mentioned. The Hπ structures for the concentration of species X are the first to appear until they lose their stability to stripes (see inset of Figure 4). However if one further increases μ, surprisingly the stripes then give way to a branch of H0 solutions (*reentrant hexagons*) also giving rise to a new hysteresis loop. We thus have the succession Hπ, Hπ/S, S, S/H0, H0 (where A/B indicates bistability of structures A and B) when the bifurcation parameter increases (Figure 4). A similar phenomenon takes place in the Schnackenberg [41] and other models. The origin [46] of this feature lies in the structure of the quadratic coupling intensity v that contains a renormalization factor proportional to μ. Indeed $v = v_0 + \alpha\mu$. For $\mu \to 0$, the

dominant term is v_0 (< 0) giving rise to Hπ structures. However, because the coefficient α (that is system-dependent) is positive and sometimes large, as in the Brusselator, the corrective term soon grows as μ increases. Eventually the sign of the quadratic coupling is reversed and this leads to an exchange of stability between the two types of hexagons. The stability of the stripes with respect to the hexagons is also modified leading to the scenario given in Figure 4 for the Brusselator. A complete analysis was carried through for the Schnackenberg model [39] leading to the following possible scenarios that had been discovered in the numerical simulations [42] of this model: Hπ, Hπ/S, S, S/H0, H0 (as above); S, S/H0, H0; H0,H0/S, S, S/H0, H0; H0, H0/S, H0; H0.

Interestingly, the complete scenario represented for the Brusselator in Figure 4 seems to have been observed experimentally in the CIMA reaction [47].

Higher order ($M > 3$) superpositions of active modes, yielding multiperiodic patterns are also possible [48]. Some have been analyzed in relation to quasicrystallinity [49] and 'turbulent' crystals ($M \to \infty$) [37, 50]. As they have been reported neither in experiments nor in numerical simulations on chemical systems we will not discuss them further.

3.2.3. Space Dimension = 3

Many experimentally obtained Turing patterns are truly 3D [19, 51] and one thus has to study the pattern selection in that case by proceeding along the same lines as before [38, 52]. The orientational degeneracy now tells us that all modes on the *critical sphere* $|\mathbf{k}| = k_c$ may become active.

The general structure of the amplitude equations is now

$$
\begin{aligned}
\frac{\mathrm{d}A_i}{\mathrm{d}t} =\ & \mu A_i + v \sum_j \sum_k A_j^* A_k^* \delta(\mathbf{k_i} + \mathbf{k_j} + \mathbf{k_k}) \\
& - g_D |A_i|^2 A_i - \sum_{i \neq j} g_{ND(ij)} |A_j|^2 A_i \\
& - \sum_j \sum_k \sum_m l(jkm) A_j^* A_k^* A_m^* \delta(\mathbf{k_i} + \mathbf{k_j} + \mathbf{k_k} + \mathbf{k_m})
\end{aligned}
\tag{28}
$$

where here also the couplings $g_{ND}(ij)$ and $l(jkm)$ are functions of the angles between the wavevectors of the chosen set of M pairs of active modes. The $l(jkm)$ couplings arise from subsets of the active wavevectors forming noncoplanar closed loops with $\mathbf{k_i}$.

The case $M = 1$ again corresponds to a pattern periodic in one direction. It is the natural 3D extension of the 2D stripes and thus consists of a smectic-like

ordering of lamellae (lam). Their amplitude equation is identical to Equation (21) and thus in Equation (28) $v = g_{ND}(ij) = l(jkm) = 0$.

Similarly the $M = 2$ case is also the 3D extension of the squares ($v = l(jkm) = 0$). It consists of two orthogonally intersecting sets of lamellae corresponding to prisms with a square section when this section is made perpendicularly to $\mathbf{k}_1 \times \mathbf{k}_2$. They are also unstable when $g_D < g_{ND}$.

For $M = 3$, along the same line we may obtain hexagonally packed cylinders (hpc) of type π or 0 depending on the sign of v but $l(jkm) = 0$.

However, as soon as $M \geq 3$ all the space tessellations enter the selection game and one can draw on the results of standard crystallography to sort things out. Indeed for $M = 3$, one may chose the three pairs of wavevectors along the coordinates triad thereby obtaining a structure where the maxima of concentration lie on the vertices of a simple cubic (sc) lattice ($v = 0$ but $l(jkm) \neq 0$). For $M = 4$ the vectors characterizing the active modes may be chosen as the basic vectors of a body centered cubic lattice in k-space (reciprocal space). This then yields a structure in physical space where the maxima of concentration form a face centered cubic (fcc) lattice ($v = l(jkm) = 0$). On the contrary, for $M = 6$, the chosen vectors may be those of a fcc reciprocal lattice. In reciprocal space these six pairs of wavevectors may be arranged on the edges of a regular octahedron. Each active mode is involved in two resonant triads ($v \neq 0$). In real space it gives rise to a body centered cubic lattice (bcc).

For $g_D < g_{ND}$ and in the weakly nonlinear theory (equivalent to the 2D hex-stripes competition and thus negligeable v renormalization) the stability study leads to sc and fcc structures unstable with respect to the bcc, hpc and lam patterns. Thus, on increasing μ the bcc structure is the first to appear subcritically; it is followed, also subcritically by the hpc pattern that finally yields to the lamellae. On reversing the variation of the bifurcation parameter one backtracks through these structures with the corresponding hysteresis loops. These structures have been observed, in that order, in numerical simulations of the Brusselator [52]. There is also experimental evidence for the bcc and hpc patterns [51].

Although no systematic analytical or numerical studies have yet been undertaken, the renormalization of the quadratic coupling will also lead to reentrant hpc and bcc structures thereby giving rise to a host of modified bifurcation diagrams. Also other values of M should give rise to 3D quasicrystalline patterns.

4. Phase Dynamics and Pattern Selection in the Sidebands

Until now the discussion of pattern selection has been centered on the stability of structures built solely with critical modes ($|\mathbf{k}| = k_c$). The effects of

the modes in the sidebands have to be analyzed starting from the envelope amplitude equations (Equation (18)) that were derived for this purpose. As results exist only in 2D the discussion will be restricted to this case. The 3D situation will be commented upon at the end.

Consider first the striped patterns ($M = 1$) for which Equation (18) is simply (Newell–Whitehead–Segel equation)

$$\frac{\partial A}{\partial t} = \mu A - |A^2|A + \left[\frac{\partial}{\partial x} - \frac{i}{\sqrt{2\pi}}\frac{\partial^2}{\partial y^2}\right]^2 A \tag{18'}$$

where the variables have been scaled to get rid of the unimportant constants.

This equation possesses a one-parameter family of stationary solutions representing all the stripes with wavevectors belonging to the sidebands [2]:

$$A_Q = \sqrt{\mu - Q^2}\, e^{iQX} \qquad (\mu > Q^2) \tag{29}$$

where Q is the wavenumber (see Equation (11)) that is proportional to $\mathbf{k} - \mathbf{k}_c$. To study the stability of this set of solutions it may be assumed that A would be of the form

$$A = \left(\sqrt{\mu - Q^2} + u\right) e^{[iQX + \phi(X,Y,T)]}. \tag{30}$$

Linear stability analysis then yields a *phase diffusion equation* [2, 28, 53] for the slow phase modulations $\phi(X, Y, T)$ that evolve on time and length scales larger than those of the modulus of A:

$$\frac{\partial \phi}{\partial T} = \mathcal{D}_x \frac{\partial^2 \phi}{\partial X^2} + \mathcal{D}_y \frac{\partial^2 \phi}{\partial Y^2} \tag{31}$$

$$\mathcal{D}_x = \frac{\mu - 3Q^2}{\mu - Q^2}, \qquad \mathcal{D}_y = \sqrt{\frac{2}{\pi}}\, Q, \tag{32}$$

where the gradient, $\nabla \phi$, of the phase represents the local wavevector.

When $\mathcal{D}_x$ and $\mathcal{D}_y > 0$, Equation (31) implies that the longitudinal and transverse ($\mathbf{k}_c + \mathbf{Q}$ lies along x!) modulational perturbations will relax by a diffusive like process and in the end straight stripes will be recovered. On the contrary negative *phase diffusion coefficients* signify a *phase instability*: (i) $\mathcal{D}_x < 0$, the *Eckhaus instability* that is a special case of the universal Benjamin–Feir instability. It plays for the Turing patterns a role similar to the phase instability of the limit cycle resulting from a Hopf bifurcation. Modulations parallel to the axis, compression and dilation, of the stripe pattern might occur. (ii) $\mathcal{D}_y < 0$, the *zig-zag instability*: modulations perpendicular to the axis may grow and undulated stripes might be generated.

Such instabilities will result either by applying a perturbation with an improper wavenumber to the stripes or if the initial stripes have a wavelength that lies outside the $(\mathcal{D}_x, \mathcal{D}_y > 0)$ band. As usual, to assess the outcome of such instabilities, one has to include the nonlinear contributions in the phase diffusion equations. This can be done without conceptual difficulties by standard techniques. We will however not write down such contributions explicitly here. Indeed this subject has recently been reviewed [54]. Let us merely note that if those nonlinear couplings may saturate the instabilities then modulated patterns are stabilized: respectively periodically dilated/compressed or undulated stripe patterns (as those that were discovered in the bifurcation diagram for the Brusselator for a wide region of values of B [40]). On the contrary, when the instabilities are not saturated the phase gradients then grow without bounds and the phase description breaks down. One then has to return to the full amplitude equations to take into account that the modulus of the amplitude jointly becomes depressed and even zero at those phase singularity points (phase-slips) [54]. This often leads to wavenumber changing processes giving rise to new sets of straight stripes with a wavelength again inside the stable $(\mathcal{D}_x, \mathcal{D}_y > 0)$ band. The conditions $(\mathcal{D}_x, \mathcal{D}_y > 0)$ therefore select a subset of stable stripes (Figure 5a).

Eckhaus and zig-zag instabilities also play a predominant role in the phase stability of square patterns $(M = 2)$ [55]. However, as this type of structure is not expected in chemical systems (because usually $g_D < g_{ND}$) its phase instabilities will not be discussed further here.

Before discussing the phase dynamics for the $M = 3$ case we want to exercise a word of caution regarding the aspect of the related patterns. As soon as modes in the sidebands become excited, the resonant condition $k_1 + k_2 + k_3 = 0$ may be satisfied with two or even three wavevectors whose lengths differ from k_c by an amount proportional to $\sqrt{\mu}$ and forming angles that are also slightly off $\pi/3$. For polygonal patterns the sidebands thus lead to an allowed band of angles. In those cases one obtains 'nonequilateral' hexagonal patterns that have the geometrical appearance of rhombs [56]. Contrary to rhombs mentioned before $(M = 2)$ they will however exhibit three basic peaks of unequal intensity in their Fourier spectrum. Such deformations are favored when the hexagonal pattern has to adapt to stresses related to boundary conditions (e.g. periodic conditions in a square system in numerical simulations) or to defects such as grain boundaries in extended system. On the other hand it is worthwhile noticing that nonvariational effects may help stabilize the mixed modes with $k \neq k_c$ between hexagons and stripes [57].

The linear phase diffusion equations have also been derived for patterns of hexagonal symmetry $(M = 3)$ [58, 59] for a variational model (otherwise
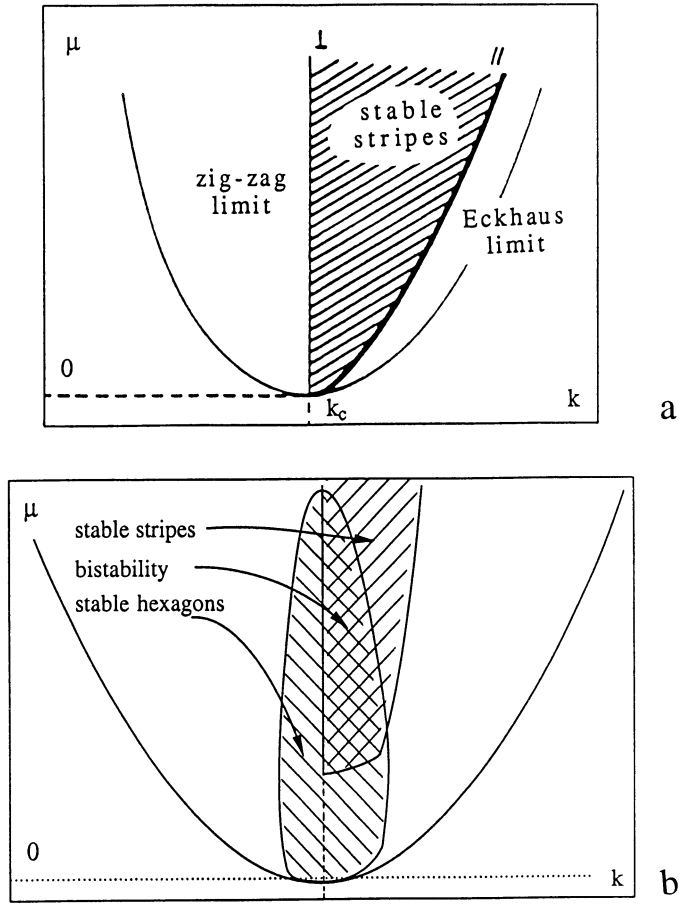
Fig. 5.   Bifurcation diagrams in the control parameter (μ)/wavenumber (k) representation showing the results of the stability analysis in the sidebands of active modes: (a) the Eckhaus and zig-zag instability reduce the band of stable stripes to the hatched 'tong'; (b) their own phase instabilities lead to similar effects for the patterns of hexagonal symmetry. The reduced stripes domain (cf. (a)) is also represented.

nonvariational contributions may lead to supplementary terms). The phase is here a two-dimensional vector and the phase equation reads

$$\frac{\partial \bar{\phi}}{\partial T} = \mathcal{D}_\perp \nabla^2 \bar{\phi} + (\mathcal{D}_\parallel - \mathcal{D}_\perp)\bar{\nabla}(\bar{\nabla} \cdot \bar{\phi}) \tag{33}$$

$$\mathcal{D}_\perp = k_c^2 + 6kk_c - [16k^2k_c^4/2(g_D - g_{ND})R^2 + 4vR]$$

$$\mathcal{D}_\parallel = 3k_c^2 + 10kk_c - 16k^2k_c^4 \left\{ [1/2(g_D - g_{ND})R^2 + 4vR] \right.$$

$$\left. + [1/2(g_D + 2g_{ND})R^2 - 2vR] \right\} \tag{34}$$

where R is the modulus of the amplitude of the hexagons. Here again the hexagonal planforms with $|\mathbf{k}| \neq k_c$ are only stable in a closed domain defined by $\mathcal{D}_{\parallel} > 0$ and $\mathcal{D}_{\perp} > 0$ (Figure 5b). The domain is closed because, at higher μ, the hexagons become unstable with respect to stripes. The stability limits have also been tested numerically as well as the relaxation of unstable hexagonal patterns towards patterns with stable wavelengths. For the scenario involving reentrant hexagonal structures, the tong of stable stripes will also be closed from above due to the existence of the hexagons with the other total phase value.

It is interesting to compare [26] the phase dynamics, Equations (31) and (33), with the equation of motion of the displacement field $\bar{\mathbf{u}}$ of an isotropic solid [60]

$$\rho \frac{\partial^2 \bar{\mathbf{u}}}{\partial t^2} = \mu \nabla^2 \bar{\mathbf{u}} + (\lambda + \mu) \bar{\nabla} (\bar{\nabla} \cdot \bar{\mathbf{u}}) \tag{35}$$

where μ and λ are the Lamé coefficients. Hence the phase diffusion coefficients of the variational model play a role similar to the elasticity coefficients of a solid, but the phase dynamics is diffusive and not propagative. This analogy and difference allow one to apprehend the structure of the phase diffusion equations in 3D for variational models.

Because they reduce the allowable band of wavenumbers, the phase diffusion instabilities provide a *wavelength selection* mechanism. However, it is not totally determined and the selected wavelength may therefore depend on the characteristics of the nucleation of the structure: if it develops from a random background noise applied to the unstable reference state it is in general different from that appearing beyond a front invading this unstable state.

Although the derivation of the phase equations has been sketched in the weakly nonlinear regime, i.e. starting from the amplitude equations, they are far more general and may be derived far from the onset of the structures. The starting point is then the finite amplitude planform the wavevectors of which are allowed to vary slowly over the extent of the reactor. In this context, that follows the work of Witham on nonlinear wavetrains, the phase diffusion equations appear as solvability conditions [28, 61].

The large aspect ratio experimental 2D Turing structures, that arise through amplification of various initial nonuniform biases, usually exhibit a very patchy appearance with many defects (Figure 6). Indeed the combination, on the one hand, of the rotational invariance that allows all orientations of a given pattern on equal footing and, on the other hand, the boundary conditions that choose its orientation locally (frustration), act together to give rather complicated *textures*. These consist of randomly oriented domains separated by grain boundaries and containing defects (dislocations, disclinations, foci, spirals,
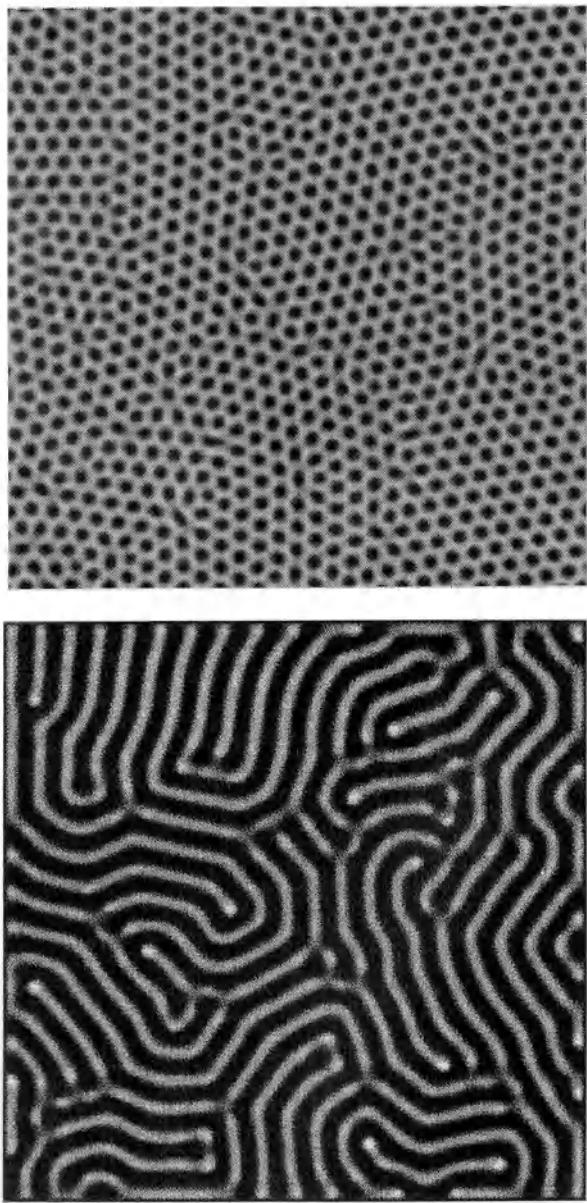
Fig. 6. Large aspect ratio Turing patterns for the Brusselator of hexagonal and stripe symmetry exhibiting defects and grain boundaries. The representation is as in Figure 3.

...) that play an important part in the pattern properties and its dynamics. The phase equations constitute the privileged formalism to study the dynamics of these defects [62] that riddle the large aspect ratio experimental quasi-2D

Turing patterns. In 3D, the orientational effects of the feeding ramps tend to prevent the formation of most defects. The study of such 3D defects, some of which undoubtedly will show some similarity with the defects of solid state physics (screw dislocations for instance), but also spherical foci and scrolls, has not yet been undertaken in the context of space symmetry-breaking driven systems.

5. Localized Patterns

Until now we have only considered *global* structures that occupy the whole space where the species are allowed to diffuse and react. *Localized* structures in the form of coexisting states have also been obtained in the experiments and numerical simulations. We must however distinguish between two types of such structures: (i) those appearing in the presence of nonuniformly distributed constraints, and (ii) those which may be generated in a uniform environment by a localized perturbation.

5.1. RAMPED TURING STRUCTURES

In most experimental designs and in many biological problems the system is kept under control by feeds through its boundaries that induce specific nonuniformities. We now consider the effects of such spatial variations on chemical dissipative structures.

   The theoretical analysis of this type of problem has been initiated in the case of the one-dimensional Brusselator model when the species A that may determine the instability thresholds varies in space and presents a local minimum at position x^*. Such profiles give rise to structures confined in the vicinity of this most unstable region with an exponentially decaying amplitude as the reference state regains stability [1, 63, 64]. These structures thus determine the extent of their region of existence that may remain far from the boundaries of the reactor. For such ramps, the bifurcation is perfect but is delayed with respect to the uniform conditions [65]: the supercritical region must be sufficiently large so that at least one wavelength may fit in. This shift allows one to understand the orientational effect of such ramps in 2D [66,67]. The longitudinal stripes, with $k \perp G$ – the direction of the gradient (and the ramp) will be denoted by G – are the first to appear because they are not sensitive to such geometric constraints. When the excited domain is larger, spatial coexistence of patterns of different symmetries becomes possible [40].

   In order to assess more precisely the effects of concentration profiles on the pattern selection problem discussed in Section 3, situations where the bifurcation parameter presents a linear ramp were also considered. In one-dimensional systems ($k \parallel G$), if the control parameter is subcritical in part of

the system then the width of the sidebands of stable wavevectors is reduced [68] and in the limit of infinitely slow variation it shrinks to a single line and the wavelength is then perfectly selected. Some of these results were verified experimentally in the case of hydrodynamic instabilities [69]. The situation is however much more complicated in 2D (or 3D) when bands of various orientations and polygonal structures compete.

Theoretical studies show that in infinite 2D systems, slow monotonous ramps of overcriticality select longitudinal ($\mathbf{k} \perp \mathbf{G}$) stripes [70]. Therefore the wavelength selection mechanism discussed above does not apply in 2D [71].

In any finite container, where the bifurcation parameter is a monotonic function of a horizontal coordinate, the system is most unstable adjacent to the endwall perpendicular to the profile. In order to investigate the orientational effect of such endwalls the equations of the Brusselator model have been solved numerically [40] in a rectangular domain with a linear ramp of B: $B(x) = B(0) + \beta x$ ($0 \leq x \leq L$). No flux boundary conditions are imposed along the sides perpendicular to the ramp and periodic boundary conditions apply along the others. In this case the boundary conditions are not satisfied exactly by the basic state which holds prior to the onset of the Turing instability $X_b = A$; $Y_b = B(x)/A$. We have indeed $\partial Y_b/\partial x = \beta \neq 0$ ('imperfect' problem [72]). This discrepancy induces a forcing of the basic solution which tends to favor transverse stripes with their axis parallel to such walls. In a simulation where the conditions are such that the whole system is supercritical, transverse stripes ($\mathbf{k} \parallel \mathbf{G}$) indeed appear near the endwalls whereas longitudinal stripes are selected in the middle of the container. In smaller systems, but for the same value of β, the orientational influence of the boundaries becomes dominant and the transverse stripes invade the whole system. In the 'perfect' problem, i.e. when the basic solution satisfies the boundary conditions, $\partial Y_b/\partial x|_{0,L} = \beta$, only longitudinal stripes are selected by the ramp [73].

When patterns of different symmetries coexist spatially along the ramp various contradictory orientational effects are simultaneously at play. Considering again the same model we now apply $B = B_c$ at the grid point $x = L/3$ to include a subcritical region (Figure 7). Starting with $B(L) = 7$ with random initial conditions one obtains a hexagonal pattern (Hπ with $\mathbf{k}_1 + \mathbf{k}_2 + \mathbf{k}_3 = 0$ and $\mathbf{k}_1 \perp \mathbf{G}$) which invades the subcritical domain. In the region straddling B_c one finds amplitude variations characteristic of imperfect bifurcations. Such bifurcations have been predicted theoretically in the present context for roll structures in weak linear ramps. We then proceed by making a series of quasistatical increases of $B(L)$ and thus of the ramp. At $B(L) = 8.2$, the stripes that enter the show appear near the endwall at $x = L$ with $\mathbf{k} = \mathbf{k}_2$ (or $\mathbf{k}_3$) implying an orientational effect of the domain wall between the hexag-
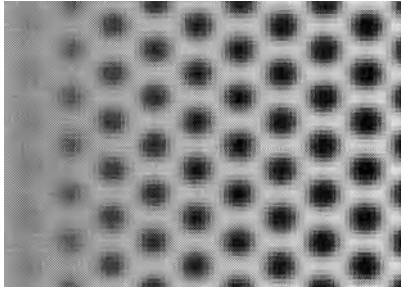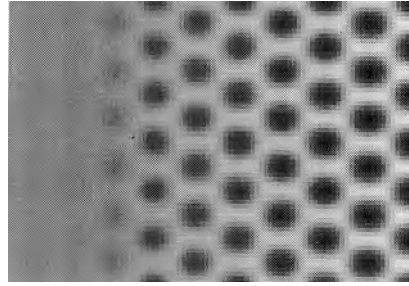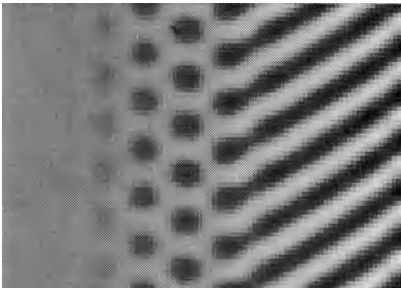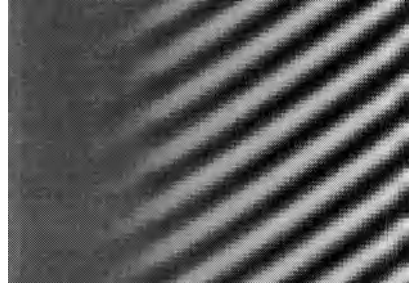
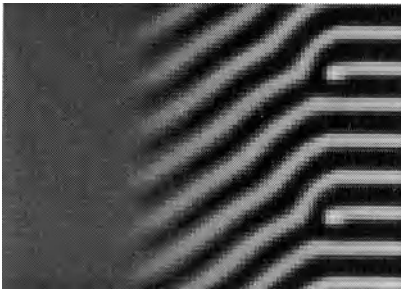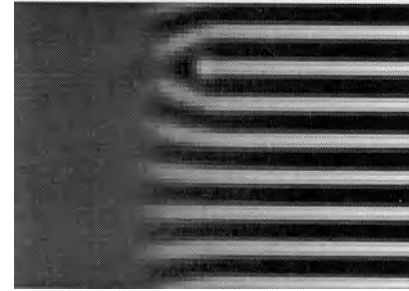[a] B_L=7.0   [b] B_L=8.0

[c] B_L=8.2   [d] B_L=10.0

[e] B_L=16.0 t_1 [f] B_L=16.0 $t_2 > t_1$

Fig. 7. Turing patterns for the 2D Brusselator (parameters as in Figure 4) in a linear ramp of the bifurcation parameter B for a system of size $L \times L'$. The values B_c and B_L are respectively applied at positions $L/3$ and L. Pattern (a) is obtained from random initial conditions while the others are formed by increasing B_L quasistatically from the preceding stationary pattern. (e) and (f) are for the same conditions but at two successive times. The representation is as in Figure 3.

onal structure and the stripes. At this stage we have the unfolding in space of the bifurcation diagram. Each pattern develops in the region where the local value of the bifurcation parameter allows it to be stable. The gradient

of course shifts the stability boundaries with respect to the corresponding uniform problem. The new oblique stripes are drifting perpendicularly to $\mathbf{G}$ at constant velocity because of the presence of periodic boundaries in that direction. This is the sign that a parity-breaking bifurcation with respect to the direction of the gradient has occurred. The $H\pi$ are entrained in this motion. For $B(L) = 10$ the $H\pi$ are in the process of being squeezed out because the gradient is now so large that they have less than one wavelength to fit into. As soon as they have vanished a set of longitudinal rolls starts to invade the system from the $x = L$ border. No H0 intervene because of the quasistatical nature of the procedure.

Many numerical experiments with ramps lead to patterns containing a lot of bent stripes and defects probably because of the ubiquitous presence of undulated stripes that are stable for a wide range of values of B, as was mentioned before.

These examples clearly show that pattern selection becomes indeed very complicated even in the presence of the simplest form of profile. The slope of the ramp, the boundaries, and the domain walls all compete to determine the selected orientation of the patterns resulting in a large multiplicity of localized structures.

Finally, in the presence of a very localized inhomogeneity, reaction-diffusion systems can develop local periodic undulations under far less restrictive conditions than for the onset of global patterns [74]. Such undulatory inhomogeneities can for instance occur in the vicinity of a catalyst particle even though no instabilites can be found in the corresponding homogeneous system. As a result, non trivial cooperative phenomena may arise in arrays of catalytic sites which could play an important role in heterogeneous catalysis and in biological systems containing immobilized enzymes [75].

5.2. Pinning and Intrinsic Localized Structures

In Section 3 we have shown that diffusion-driven instabilities can give rise to numerous examples of multistability. Under such circumstances the system may also exhibit localized structures corresponding to the spatial juxtaposition of the various stable states. As mentioned in Section 3.1 some stabilization mechanism must intervene. We first describe the patterns that may appear in the 1D Lengyel–Epstein model in the range of values of parameters for which the Turing instability is subcritical [43].

The simplest consists of a front (kink) connecting a Turing pattern to the HSS (Figure 8a). Because in the simulations the hysteresis region is rather large this front is sharp and it can thus interact with the underlying Turing pattern leading to the pinning of the interface by the structure [29] (Section 3.1.3). As a result the front velocity is zero in a finite range of values
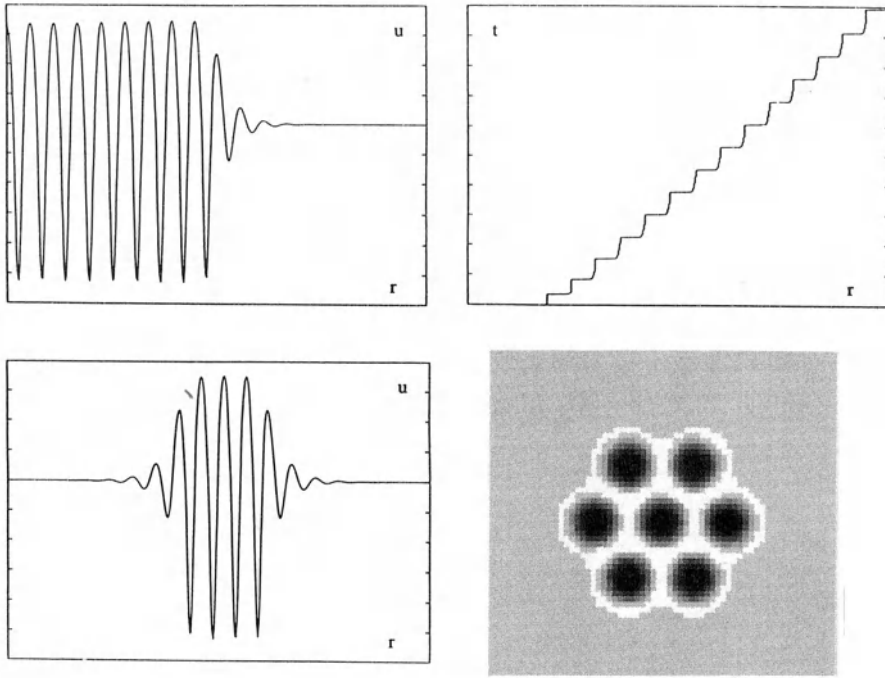
Fig. 8.   Intrinsic localized patterns for the concentration of variable u ($\equiv [I^-]$) in the Lengyel–Epstein model for values of the parameters (see [43]) such that the stripes also appear subcritically (cf. Equation (23)): (a) pinned front between a 1D Turing pattern and the uniform reference state; (b) position of the front with respect to time, outside but close to the edge of the pinning band; the nonuniform character of the velocity of a 'freezing' front is clearly observed; (c) stable, pinned, 1D droplet of Turing state embedded in the background of the stable uniform reference state: (d) stable, pinned, 2D droplet of the hexagonal structure enclosed in the stable uniform reference state.

of the parameter B. Outside this locking band one observes a depinning transition; the structure invades the territory of the HSS, for $B < B_{low}$ (solidification front) and the reverse situation occurs for $B > B_{high}$ (fusion front). In this process the displacement of the front is not uniform but proceeds by jumps of one wavelength of the underlying created structure (Figure 8b). The time interval between successive jumps increases when the pinning band is approached from the outside (plateau behavior) in such a way that the mean velocity of the front goes to zero at the pinning limit. This phenomenon of interface pinning results from *nonadiabatic effects* that are not included in the standard amplitude equations of the weakly nonlinear·theory [76, 77]. Such interferences between a kink and a structure that have also been obtained in an hydrodynamical system [78], are frequent in condensed matter physics where they are known to dominate the dynamics of dislocations, charge density waves or magnetic domains [79].

These fronts also furnish the building blocks for the construction of coherent structures formed by droplets of one state embedded in another. Simulations have indeed produced localized Turing structures [43] limited to a few wavelengths appearing in an otherwise uniform background (Figure 8c). Depending on the initial conditions, such localized states with different numbers of wavelengths in the core have been obtained for the same values of the parameters. This multistability is mostly the consequence of the domain wall pinning effect (not of nonvariational effects) as the width of the locking band is the same for the various localized patterns as for the front. The complementary coherent structure where a bubble of the HSS appears in a Turing background has also been obtained.

In 2D, in the subcritical region, the system may exhibit tristability between $H\pi$, stripes and the HSS [43]. As a result a large variety of 2D localized structures is possible. The pinning of a structure is more efficient when the wavevectors characterizing the pattern are nearly perpendicular to the domain boundary. This condition determines the shape and the growth mechanism of the localized structures. An hexagonal localized domain of hexagons embedded in the HSS has for instance been obtained (Figure 8d). Isolated patches of hexagons have also been observed in the case of strong resonant forcing of oscillators [80] and in experiments on thermocapillary convection [81]. In the region where they are both stable a band of stripes sandwiched between two domains of hexagons or the opposite may also occur [43].

6. Conclusions and Outlook

The results discussed above show that new progress has indeed been made in the understanding of the properties of large aspect ratio Turing patterns in relation with the recently obtained experimental results.

As a matter of conclusion, we wish to consider aspects that have also been tackled but need further consideration before a complete picture will be available.

Unslaving of the harmonics: The width of the sidebands grows either when the control parameter B increases or if the curvature, as a function of the wavenumber, at the maximum of the linear critical frequency becomes smaller, for instance as the ratio D_a/D_h decreases. Then overtones of the critical modes, that were otherwise slaved, progressively rejoin the active set of modes and their resonant interactions with the fundamental modes must be taken into account. This effect also grows more important as the space dimension of the pattern increases. Indeed for a periodic structure in one dimension the first harmonic to become excited lies at $k = 2k_c$, whereas for patterns of hexagonal symmetry that are periodic in two dimensions the first overtone is at $k = \sqrt{3}\, k_c$. Further, for 3D patterns they appear

already at $k = \sqrt{(4/3)}\, k_c$ (fcc). As a result not only can structures with new symmetries come into play and compete with those already defined earlier but the stability of previously considered patterns may also be modified. This brings noteworthy modifications to the bifurcations diagrams.

As the simplest exemple one may consider the case of a 1D striped pattern. In deriving the amplitude equations, the concentrations are now expanded as

$$\varepsilon \mathbf{C}_1 = \left[\mathbf{E}_{\mathbf{T}_1} A_1(T)\, e^{i\mathbf{k}_1 \cdot \mathbf{r}} + \mathbf{E}_{\mathbf{T}_2} A_2(T)\, e^{2i\mathbf{k}_1 \cdot \mathbf{r}} + c \cdot c \right] \tag{36}$$

where A_1 and A_2 are respectively the amplitudes of the critical mode and its first overtone. The amplitude equations are readily obtained

$$\frac{dA_1}{dt} = \mu_1 A_1 + h_1 A_1^* A_2 - g_D |A_1|^2 A_1 - g_{ND} |A_2|^2 A_1$$

$$\frac{dA_2}{dt} = \mu_2 A_2 - h_2 A_1^2 - g_D |A_2|^2 A_2 - g_{ND} |A_1|^2 A_2 \tag{37}$$

where μ_h is the distance from criticality of the overtone and as usual the values of the coefficients depend on the particular model studied. These equations have been analyzed in the context of a convection problem [82] where it has been shown that besides steady 'roll'-type convection (the equivalent of the stripes), travelling and standing waves are now also possible.

Similarly in 2D for patterns of hexagonal symmetry, besides the basic triad of modes $\{\mathbf{k}_1, \mathbf{k}_2, \mathbf{k}_3\}$, one has to take into account the resonant coupling with the first overtone triad $\{\mathbf{K}_1 = \mathbf{k}_2 - \mathbf{k}_3, \mathbf{K}_2 = \mathbf{k}_3 - \mathbf{k}_1, \mathbf{K}_3 = \mathbf{k}_1 - \mathbf{k}_2\}$. We will not write down the twelve coupled amplitude equations that result. New possible structures are shown in Figure 9 and presents some similarities with the 'black eyes' structures obtained in the CIMA reaction [47]. Let us also mention that the square patterns may now also be made stable.

However, the greatest novelty arises in 3D. Indeed besides the fact that the fcc and sc structures may now be made stable in some region of the bifurcation diagram [83], structures of a totally different geometrical nature are now possible. Some results have indeed become available in the field of microstructured fluids and particularly in the study of phase stability of diblock copolymer systems [84] that present competition between structures similar to that encountered in 3D Turing variational patterns. Indeed they also exhibit lam, hpc and bcc structures. However it has also been shown that these polymers may organize in a bicontinuous double-diamond (bdd) structure [85]. There one component resides in two intertwined but distinct labyrinthine networks, each exhibiting diamond cubic symmetry, while the other component lies in the continuous matrix between the two diamond channels. The complicated interlocking surface separating the components has the property of minimizing its area relative to the volume it encloses and
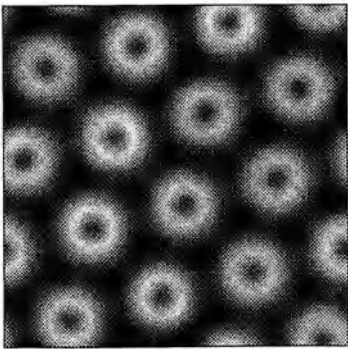
(a)
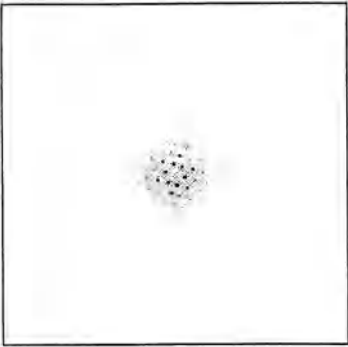
(b)
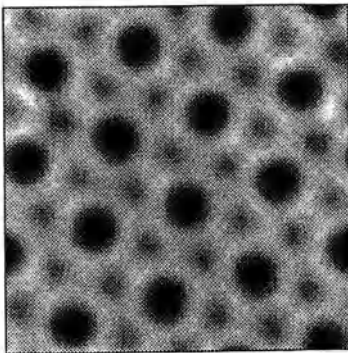
(c)

Fig. 9.   (a) and (c): Two Turing structures model of hexagonal symmetry, obtained with the Brusselator model, where the overtones have been activated as is attested by the Fourier transform (b). (a) bears some resemblance with the experimental 'black eyes' structures.

constitutes a so-called triply periodic minimal surface [86], an object of great mathematical curiosity that is thought to find applications in various branches of physical chemistry [87, 88]. It is interesting to mention that this bdd and the bcc structure have the same basic wavevectors but that they differ in the choice of the excited overtones [89]. It is, however, not yet completely clear if the excitation of these harmonics is sufficient to explain the stabilization of such a bdd pattern. The conditions for obtaining Turing structures with such symmetries have however not yet been established. In such a context a doubly periodic $\pi/2$ twist boundary between lamellar domains [85], that corresponds to the classically known first kind Scherk surface, would qualify as a new kind of defect. Such defects have been obtained in a 3D simulation of the Brusselator model [90].

Degenerate bifurcations: In the vicinity of degenarate bifurcation points, i.e. bifurcations with higher codimension, one must also study the coupling and competition of the Turing active modes with the active modes characterizing the competing bifurcation. It has recently been shown experimentally [91], on the CIMA reaction, that unfolding around a Turing–Hopf codimension 2 point can be carried out by varying the concentrations of two independant chemical species: the malonic acid and the starch color indicator that also complexes the I_3^- ions. One then goes over from stationary Turing structures to wave patterns characteristic of a simple oscillatory regime in agreement with the Hunding–Sorensen–Lengyel–Epstein mechanism [92, 93].

Near such a codimension 2 point the concentration fields may be written as

$$\varepsilon \mathbf{C}_1 = \left[\mathbf{E_T} A_T(T)\, e^{i k_i \cdot r} + \mathbf{E_H} A_H(T)\, e^{i\omega t} + c \cdot c \right] \tag{38}$$

where $\mathbf{E_T}$ and $\mathbf{E_H}$ are the critical Turing and Hopf eigenvectors of the linearized reaction-diffusion operator. The resulting envelope amplitude equations (in 1D) then read [91, 94, 95]

$$\frac{dA_T}{dt} = \mu_T A_T - g_{TT}|A_T|^2 A_T - g_{TH}|A_H|^2 A_T + D_T \frac{\partial^2 A_T}{\partial x^2}$$

$$\frac{dA_H}{dt} = \mu_H A_H - (\beta_r + i\beta_i)|A_H|^2 A_H$$

$$- (\delta_r + i\delta_i)|A_T|^2 A_H + (D_{H,r} + iD_{H,i})\frac{\partial^2 A_H}{\partial x^2}. \tag{39}$$

Standard amplitude equations have also been derived for 1D [96] and 2D [97] systems.

Three types of solutions result: pure Turing or Hopf modes or mixed modes representing oscillating Turing patterns. Two classes of competition may then occur according to the stability of the mixed modes. If they are unstable

$(\beta_r g_{TT} - \delta_r g_{TH} < 0)$ then there exists a region of bistability between the Turing and Hopf modes in the bifurcation diagram. On the contrary when $(\beta_r g_{TT} - \delta_r g_{TH} > 0)$ the domains of stable Turing and Hopf modes are connected by a domain where only the mixed mode is stable. For each of these classes a very large number of scenarios are possible depending on either, whether the Turing or Hopf bifurcation comes first, or whether the bifurcations are super- or subcritical.

Recently two particular effects have been studied. When the mixed mode is unstable, in the region where Turing and Hopf modes coexist (bistability) localized structures (cf. Section 5.2) have been obtained [91]. In 1D, the simplest consist of a stationary front, stabilized by pinning and nonvariational effects, separating in space the region where the Turing mode dominates from the region where the Hopf mode reigns. Its aspect is that of a Turing structure emitting waves (Figure 10a). In this case also there exist depinning transitions where one state starts to invade the other (Figure 10b). However the motion of the front may now be more complex [98] than the situation discussed in Section 5.2. Such fronts may then again serve as building blocks for droplets of one state embedded in the other (Figures 10c, d). The simplest embedded Turing pulse, with the core containing the smallest number (one) of wavelengths and emitting waves on either side in phase oppostion is then similar to the 1D spiral (chemical flip-flop) recently observed experimentally in the Turing–Hopf interaction region of the CIMA reaction [91]. Similarly in 2D, a spiral with a Turing 'spot' at its core may be obtained [99] in agreement with the experimental results [100]. Turing–Hopf fronts have also been studied in an hydrodynamics [101] and in an array of resistively coupled LC-oscillators [102].

On the other hand, when the mixed mode is amplitude stable it may nevertheless undergo a Benjamin–Feir type of phase instability leading to phase or defect chaos although the adjoining Turing and Hopf modes are stable [103].

The recent simulations of Pearson [44] on a fed autocatalator [104], on the other hand stages interactions between Turing and saddle-node bifurcations or even situations where a Hopf bifurcation interacts with the two previous ones. Then a plethora of scenarios may result. However, the Turing bifurcations are genuine but they occur on the stable branch of an isola of uniform states and may exist beyond the limits of the isola.

Turing patterns interacting with flow: Recently the influence of a flow field on the Turing instability and the patterns that result have been considered [105–108]. In order not to 'scramble' the Turing patterns only flows with very weak mixing properties may be considered. A low Reynolds number flow in a tubular reactor may provide an experimental realization [109]. If the chemical reaction is passive to the flow (i.e. it does not perturb the imposed
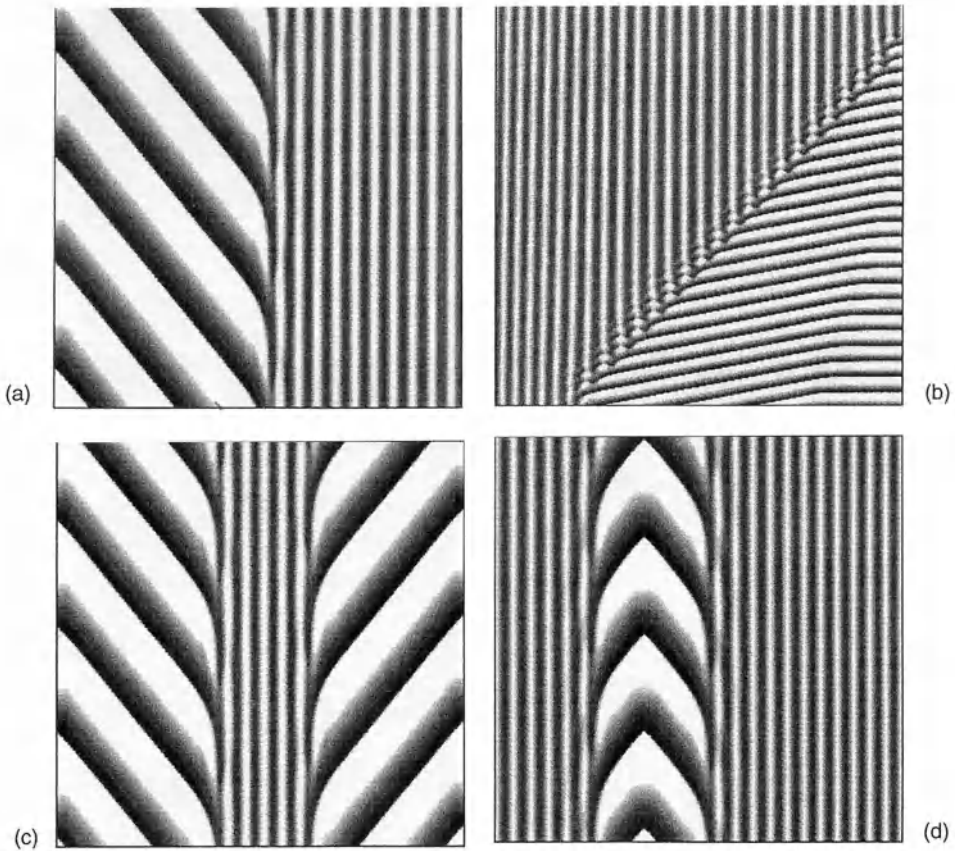
Fig. 10.   Intrinsic localized 1D Turing–Hopf patterns for the Brusselator model in a region of parameter space where the Turing and Hopf modes are bistable whereas the mixed mode is unstable. Space-time plots with time running upwards: (a) pinned front: the Turing structure emits waves into the Hopf region; (b) 'freezing' front invading the Hopf region just outside the pinning band; (c) stable Turing droplet embedded in the Hopf region; (d) stable Hopf droplet embedded in a Turing structure. For (a), (c) and (d) the parameters are the same, they differ only through the initial conditions.

velocity field, for instance by heat generation or density fluctuations), it is sufficient to include inertial flow terms $\mathbf{v} \cdot \nabla C$ in Equation (1) and analyze the resulting reaction-diffusion-convection problem.

However, due to the presence of the flow one has to distinguish, already at the level of the linear stability analysis, between *absolutely* and *convectively unstable* situations [110]. This has been overlooked in some of the recent works. In the first case, for low velocities, the perturbation grows and invades the whole reactor while the instability saturates. The resulting structures then consist of regular periodic travelling waves [105, 107]. In the other case, above a critical velocity, the perturbation grows but is advected by the flow

field so that the structure never fills the whole reactor. In a finite reactor the resulting structure is finally ejected (Figure 11). This convectively unstable state at first sight resembles the uniform reference state. However contrary to this one it is very sensitive to imperfections. Structures, similar to those arising in the absolutely unstable case, may then be generated and sustained by a noise source at some point (for instance in the entrance region) of the reactor [107, 108, 111].

The same effect seems to be at play in the case of the recently proposed DIFICI mechanism [112] of structure formation. There also the system is convectively unstable and the structure generated is advected away (except in the case of a loop reactor) [108]. The structures observed in the related experiments [113] in an open tubular reactor would thus be a noise generated pattern in a convectively unstable system.

The influence of the velocity profile of the flow (Taylor diffusion) may also lead to other interesting patterning phenomena [114–116].

Because the chemical species eventually participate in ionic form, electrical fields may also influence the patterns. The coupling of such an electrical field to the concentration has a structure similar to that of the velocity field. However, subsidiary conditions have also to be taken into account (electroneutrality, self-consistent determination of the electrical field inside the system, ...). This problem has recently been reconsidered [117].

Front structures: Instabilities induced by differential diffusion processes also play an important role in the morphological stability of fronts [118]. Consider for example a planar propagating front with a high concentration of activator and inhibitor ('activated state') behind and a low concentration of these species ahead of the wave. When the diffusion coefficients are such that $D_h \geq D_a$, a protrusion (convex in the direction of propagation) is in an advantageous position. The inhibitor leaves this zone more rapidly compared to the planar front. Thus the autocatalytic production of the activator is accelerated and the wave speed of these convex segments is increased relative to the planar wave speed. The protrusion runs forward and the curvature increases. The opposite situation arises in the concave regions. An enhanced diffusional supply of inhibitor in these regions tends to decrease the local speed of these already retarded segments. It may thus be concluded that when D_h/D_a is sufficiently large the planar front will lose stability leading to the appearance of patterned fronts or chaotic behavior. As already pointed out this mechanism has first been introduced in the study of the stability of flames [119] (leading therefore to cellular flames) although in this case convection effects are always present [120]. The stability of isothermal autocatalytic fronts in reaction-diffusion systems has also been analyzed along these lines

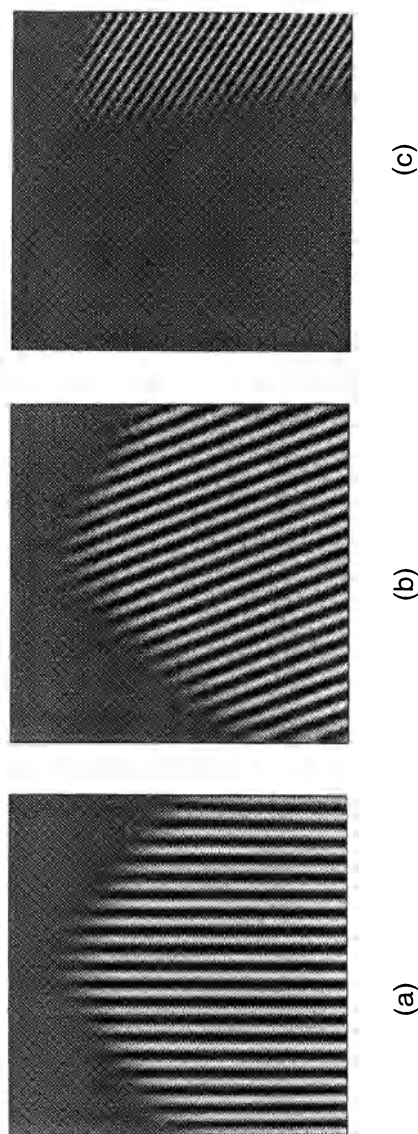(a)   (b)   (c)

Fig. 11. Absolutely and convectively unstable conditions for the generation of a 1D Turing structure in the presence of a simple flow of velocity field $\mathbf{v}(\mathbf{r}) = v_0 \mathbf{1}_x$. In the represented space-time plots (time running down vertically) the initial perturbation is at the center of the reactor. (a) $v_0 = 0$: development in time of the normal Turing structure; (b) $v_0 < v_{critical}$: the pattern develops in the whole reactor as the left front is able to proceed against the flow; because of the advection one however has a 'traveling' Turing pattern (waves); (c) $v_0 > v_{critical}$: during its growth the pattern is advected away by the flow; in a finite reactor the developing pattern eventually leaves beyond a convectively unstable state very sensitive to imperfections (noise).

[121]. Here also the intervention of an agent complexing the activator species is likely to introduce the necessary difference of diffusion coefficients.

Finally there remains to understand the origin of the recently obtained patterns [122] in the iodate-ferrocyanide-sulfite (the so-called EOE) reaction [123] generated by finite perturbations of a uniform bistable system. Do they fit in some class discussed above or are they an example of the so-called 'high amplitude' structures [27, 124–127]?

Acknowledgements

References

1. Nicolis, G. and Prigogine, I., *Self-Organization in Nonequilibrium Systems* (Wiley, New York, 1977).
2. Manneville, P., *Dissipative Structures and Weak Turbulence* (Academic Press, San Diego, 1990).
3. Kai, S., *Physics of Pattern Formation in Complex Dissipative Systems* (World Scientific, Singapore, 1992).
4. Cross, M. C. and Hohenberg, P. C., *Rev. Mod. Phys.* **65**, 854 (1993).
5. Newell, A. C. and Moloney, J. V., *Nonlinear Optics* (Addison-Wesley, Redwood City, 1992).
6. Zeldovich, Y. B., *Theory of Combustion and Detonation of Gases* (Academy of Sciences USSR, Moscow, 1944).
7. Rashevski, N., *Mathematical Biophysics* (University of Chicago Press, Chicago, 1938).
8. Turing, A., *Philos. Trans. R. Soc. Lond.* B **237**, 37 (1952).
9. Glansdorff, P. and Prigogine, I., *Thermodynamic Theory of Structure, Stability and Fluctuations* (Wiley, New York, 1971).
10. Meinhardt, H., *Models of Biological Pattern Formation* (Academic Press, New York, 1982).
11. Murray, J. D., *Mathematical Biology* (Springer, Berlin, 1989).
12. Kerner, B. S. and Osipov, V. V., *Sov. Phys. JETP* **47**, 874 (1978).
13. Willebrand, H., Niedernostheide, F. J., Dohmen, R., and Purwins, H. G., in *Oscillations and Morphogenesis*, edited by L. Rensing (Dekker, New York, 1992), p. 81.

14. Niedernostheide, F. J., Dohmen, R., Willebrand, H., Schulze, H. J., and Purwins, H. G., in *Nonlinearity with Disorder*, edited by K. Abdullaev, A. R. Bishop, and S. Pneumatikos (Springer-Verlag, Berlin, 1992), p. 282.

15. Falta, J., Imbihl, R., and Henzler, M., *Phys. Rev. Lett.* **64**, 1409 (1990).

16. Krishan, K., *Nature* **287**, 420 (1980).

17. Walgraef, D. and Ghoniem, N. M., *Phys. Rev. B* **13**, 8867 (1989).

18. Emelyanov, V. I., *Laser Physics* **2**, 389 (1992).

19. Castets, V., Dulos, E., Boissonade, J., and De Kepper, P., *Phys. Rev. Lett.* **64**, 2953 (1990).

20. Ouyang, Q. and Swinney, H. L., *Nature* **352,** 610 (1991).

21. Kerner, B. S. and Osipov, V. V., in *Nonlinear Waves I*, edited by A. V. Gaponov-Grekov, M. I. Rabinovich, and J. Engelbrecht (Springer-Verlag, Berlin, 1989), p. 126.

22. Elmer, F. J., *Physica D* **30**, 321 (1988); *Phys. Rev. A* **41**, 4174 (1990).

23. Middya, U., Sheintuch, M., Graham, M. D. and Luss, D., *Physica D* **63**, 393 (1993).

24. Bedeaux, D., Mazur, P., and Pasmanter, R. A., *Physica A* **86**, 355 (1977).

25. Ertl, G., *Science* **254**, 1750 (1991).

26. Dewel, G., Borckmans, P., and Walgraef, D., in *Chemical Instabilities*, edited by G. Nicolis and F. Baras (Reidel, Dordrecht, 1984), p. 385.

27. Kerner, B. S. and Osipov, V. V., *Sov. Phys. Usp.* **33**, 679 (1991).

28. Newell, A. C., Passot, T., and Lega, J., *Annu. Rev. Fluid Mech.* **25**, 399 (1993).

29. Pomeau, Y., *Physica D* **23**, 3 (1986).

30. Ortoleva, P. and Ross, J., *J. Chem. Phys* **63**, 3398 (1975).

31. Thual, O. and Fauve, S., *J. Phys. (Paris)* **49**, 1829 (1988).

32. Busse, F., *Rep. Progr. Phys.* **41**, 1929 (1978).

33. Malomed, B. A. and Tribelskii, M. I., *Sov. Phys. JETP* **65**, 305 (1987).

34. Epstein, I. R., Lengyel, I., Kadar, S., Kagan, M., and Yokoyama, M., *Physica A* **188**, 26 (1992).

35. Haken, H. and Olbrich, H., *J. Math. Biol.* **6**, 317 (1978).

36. Walgraef, D., Dewel, G., and Borckmans, P., *Phys. Rev. A* **21**, 397 (1980).

37. Pismen, L. M., *J. Chem. Phys.* **72**, 1900 (1980).

38. Walgraef, D., Dewel, G., and Borckmans, P., *Adv. Chem. Phys.* **49**, 311 (1982).

39. Metens, S., Dewel, G., and Borckmans, P., 'Pattern Selection in a 2D Reaction-Diffusion System', preprint (1993).

40. Borckmans, P., De Wit, A., and Dewel, G., *Physica A* **188**, 137 (1992).

41. Dufiet, V. and Boissonade, J., *J. Chem. Phys.* **96**, 664 (1992).

42. Dufiet, V. and Boissonade, J., *Physica A* **188**, 158 (1992).

43. Jensen, O., Pannbacker, V. O., Dewel, G., and Borckmans, P., *Phys. Lett. A* **179**, 91 (1993).

44. Pearson, J. E., *Science* **261**, 189 (1993).

45. Lengyel, I. and Epstein, I. R., *Science* **251**, 650 (1991).

46. Verdasca, J., De Wit, A., Dewel, G., and Borckmans, P., *Phys. Lett. A* **168**, 194 (1992).

47. Ouyang, Q., Communication at the 76th Canadian Society for Chemistry Conference, Sherbrooke (1993).

48. Walgraef, D., Dewel, G., and Borckmans, P., *Nature* **218**, 606 (1985).

49. Malomed, B. A., Nepomnyashchii, A. A., and Tribelskii, M. I., *Sov. Phys. JETP* **69**, 388 (1990).

50. Newell, A. C. and Pomeau, Y., *J. Phys. A: Math. Gen.* **26**, L429 (1993).

51. Perraud, J. J., Agladze, K., Dulos, E., and De Kepper, P., *Physica A* **188**, 1 (1992).

52. De Wit, A., Dewel, G., Borckmans, P., and Walgraef, D., *Physica D* **61**, 289 (1993).

53. Pomeau, Y. and Manneville, P., *J. Phys. Lettres (Paris)* **40**, 609 (1979).

54. Sakaguchi, H., *Progr. Theor. Phys.* **89**, 1123 (1993).

55. Hoyle, R. B., *Physica D* **67**, 198 (1993).

56. Malomed, B. A., Nepomnyashchii, A. A., and Nuz, A. E., *Physica D* **70**, 357 (1994).

57. Gunaratne, G. H., *Phys. Rev. Lett.* **71**, 1367 (1993).

58. Lauzeral, J., Metens, S., and Walgraef, D., *Europhys. Lett.* **24**, 707 (1993).
59. Sushchik, M. M. and Tsimring, L. S., *Physica D* **74**, 301 (1994).
60. Landau, L. D. and Lifshitz, E. M., *Theory of Elasticity* (Pergamon, Oxford, 1970).
61. Cross, M. C. and Newell, A. C., *Physica D* **10**, 299 (1984).
62. Passot, T. and Newell, A. C., *Physica D* **74**, 301 (1994).
63. Auchmuty, J. F. and Nicolis, G., *Bull. Math. Biol.* **37**, 323 (1975).
64. Herschkowitz-Kaufman, M. and Nicolis, G., *J. Chem. Phys.* **56**, 1890 (1972).
65. Dewel, G. and Borckmans, P., *Phys. Lett. A* **138**, 189 (1989).
66. Walton, I. C., *Quart. J. Mech. (Appl. Math.)* **35**, 33 (1982).
67. Dewel, G., Walgraef, D., and Borckmans, P., *J. Chimie Physique* **84**, 1335 (1987).
68. Kramer, L., Ben-Jacob, E., Brand, H., and Cross, M. C., *Phys. Rev. Lett.* **49**, 1891 (1982).
69. Ahlers, G., *Physica D* **51**, 421 (1991).
70. Walton, I. C., *Stud. Appl. Math.* **67**, 199 (1982).
71. Malomed, B. A. and Nepomnyashchii, A. A., *Europhys. Lett.* **21**, 195 (1993).
72. Walton, I. C., *J. Fluid Mech.* **131**, 455 (1983).
73. De Wit, A., Borckmans, P., and Dewel, G., in *Instabilities and Nonequilibrium Structures IV*, edited by E. Tirapegui and W. Zeller (Kluwer, Dordrecht, 1993), p. 247.
74. Ortoleva, P. and Ross, J., *J. Chem. Phys.* **56**, 4397 (1972).
75. Bimpong-Bota, E. K., Nitzan, A., Ortoleva, P., and Ross, J., *J. Chem. Phys.* **66**, 3650 (1977).
76. Bensimon, D., Shraiman, B. I. and Croquette, V., *Phys. Rev. A* **38**, 5461 (1988).
77. Malomed, B. A., Nepomnyashchii, A. A., and Tribelskii, M. I., *Phys. Rev. A* **42**, 7244 (1990).
78. Kolodner, P., *Phys. Rev. E* **48**, R4187 (1993).
79. Peyrard, M. and Kruskal, M. D., *Physica D* **14**, 88 (1984), and references therein.
80. Coullet, P. and Emilson, K., *Physica A* **188**, 190 (1992).
81. Gaponov-Grekov, A. V., Lomov, A. S., Osipov, G., and Rabinovich, M. I., in *Nonlinear Waves I*, edited by A. V. Gaponov-Grekov, M. I. Rabinovich, and J. Engelbrecht (Springer-Verlag, Berlin, 1989), p. 65.
82. Jones, C. A. and Proctor, M. R., *Phys. Lett. A* **121**, 224 (1987).
83. Marques, C. M. and Cates, M. E., *Europhys. Lett.* **13**, 267 (1990).
84. Leibler, L., *Macromolecules* **13**, 1602 (1980).
85. Thomas, E. L., Anderson, D. M., Henkee, C. S., and Hoffman, D., *Nature* **334**, 598 (1988).
86. Anderson, D. M., Davis, H. T., Scriven, L. E. and Nitsche, J. C., *Adv. Chem. Phys.* **77**, 337 (1990).
87. Charvolin, J. and Sadoc, J. F., *J. Physique (Paris)* **48**, 1559 (1987).
88. Andersson, S., Hyde, S. T., Larsson, K., and Lidin, S., *Chem. Rev.* **88**, 221 (1988).
89. Olvera de la Cruz, M., *Phys. Rev. Lett.* **67**, 85 (1991).
90. De Wit, A., unpublished results.
91. Perraud, J. J., De Wit, A., Dulos, E., De Kepper, P., Dewel, G., and Borckmans, P., *Phys. Rev. Lett.* **71**, 1272 (1993).
92. Hunding, A. and Sorensen, P. G., *J. Math. Biol.* **26**, 27 (1988).
93. Lengyel, I. and Epstein, I. R., *Proc. Natl. Acad. Sci. USA* **89**, 3977 (1992).
94. Kidachi, H., *Progr. Theor. Phys.* **63**, 1152 (1980).
95. De Wit, A., Ph.D. Thesis, Université Libre de Bruxelles (1993).
96. Keener, J. P., *Stud. Appl. Math.* **55**, 187 (1976).
97. Rovinsky, A. B. and Menzinger, M., *Phys. Rev. A* **46**, 6315 (1992).
98. Borckmans, P., Jensen, O., Pannbacker, V. O., Mosekilde, E., Dewel, G., and De Wit, A., in *Dynamical Phenomena in Living Systems*, edited by E. Mosekilde and O. Mouritsen (Synergetics–Springer-Verlag, Berlin) (to appear).

99. Pannbacker, V. O., Jensen, O., Mosekilde, E., Dewel, G., and Borckmans, P., in *Spatio-Temporal Patterns in Nonequilibrium Complex Systems*, edited by P. Palffy-Muhoray and P. Cladis (to appear).

100. De Kepper, P., Perraud, J. J., Rudovics, B., and Dulos, E., *Int. J. of Bifurcation and Chaos* (to appear).

101. Kolodner, P., *Phys. Rev. E* **48**, R665 (1993).

102. Heidemann, G., Bode, M., and Purwins, H. G., *Phys. Lett. A* **177**, 225 (1993).

103. De Wit, A., Dewel, G., and Borckmans, P., *Phys. Rev. E* **48** R4191 (1993).

104. Gray, P. and Scott, S. K., *Chemical Oscillations and Instabilities* (Clarendon Press, Oxford, 1990).

105. Doering, C. R. and Horsthemke, W., in *Spatio-Temporal Patterns in Nonequilibrium Complex Systems*, edited by P. Palffy-Muhoray and P. Cladis (to appear).

106. Ponce Dawson, S., Lawniczak, A., and Kapral, R., *J. Chem. Phys.* **100**, 5211 (1994).

107. Content, S., Mémoire de Licence, Université Libre de Bruxelles (1993).

108. Content, S., Dewel, G., and Borckmans, P., 'Absolute and Convective Chemical Instabilities', preprint (1993).

109. Marek, M. and Svobodova, E., *Biophysical Chemistry* **3**, 263 (1975).

110. Huerre, P. and Monkevitz, P. H., *Ann. Rev. Fluid Mech.* **22**, 473 (1990).

111. Deissler, R. J., *J. Stat. Phys.* **40**, 371 (1985).

112. Rovinsky, A. B. and Menzinger, M., *Phys. Rev. Lett.* **69**, 1193 (1992).

113. Rovinsky, A. B. and Menzinger, M., *Phys. Rev. Lett.* **70**, 778 (1993).

114. Spiegel, E. A. and Zaleski, S., *Phys. Lett. A* **106**, 335 (1984).

115. Doering, C. R. and Horsthemke, W., *Phys. Lett. A* **182**, 227 (1993).

116. Evans, G. T., *J. Theor. Biol.* **87**, 297 (1980).

117. Snita, D. and Marek, M., *Physica D* **75**, 521 (1994), and references therein.

118. Kuramoto, Y., *Chemical Oscillations, Waves, and Turbulence* (Springer-Verlag, Berlin, 1984).

119. Sivashinsky, G. I., *Ann. Rev. Fluid Mech.* **15**, 179 (1983).

120. Pelcé, P., *Dynamics of Curved Fronts* (Academic Press, San Diego, 1989).

121. Horvath, D., Petrov, V., Scott, S. K., and Showalter, K., *J. Chem. Phys.* **98**, 6332 (1993).

122. Lee, K. J., McCormick, W. D., Ouyang, Q., and Swinney, H. L., *Science* **261**, 192 (1993).

123. Edblom, E. C., Orban, M., and Epstein, I. R., *J. Am. Chem. Soc.* **108**, 2826 (1986).

124. Dockery, J. D. and Keener, J. P., *SIAM J. Appl. Math.* **49**, 539 (1989), and references therein.

125. Kness, M., Tuckerman, L. S., and Barkley, D., *Phys. Rev. A* **46**, 5054 (1992).

126. Kawczynski, A. L., Comstock, W. S., and Field, R. J., *Physica D* **54**, 220 (1992).

127. Hagberg, A. and Meron, E., *Nonlinearity* **7**, 805 (1994).

128. Pismen, L. M. and Nepomnyashchy, A. A., *Europhys. Lett.* **24**, 461 (1993).